© 2020. Published by The Company of Biologists Ltd | Journal of Cell Science (2020) 133, jcs249128. doi:10.1242/jcs.249128

RESEARCH ARTICLE

Changes in subcellular structures and states of pumilio 1 regulate the translation of target *Mad2* and cyclin B1 mRNAs

Natsumi Takei[1,*], Yuki Takada[1,*], Shohei Kawamura[1,*], Keisuke Sato[1], Atsushi Saitoh[1], Jenny Bormann[2], Wai Shan Yuen[2], John Carroll[2] and Tomoya Kotani[1,3,‡]

ABSTRACT

Temporal and spatial control of mRNA translation has emerged as a major mechanism for promoting diverse biological processes. However, the molecular nature of temporal and spatial control of translation remains unclear. In oocytes, many mRNAs are deposited as a translationally repressed form and are translated at appropriate times to promote the progression of meiosis and development. Here, we show that changes in subcellular structures and states of the RNA-binding protein pumilio 1 (Pum1) regulate the translation of target mRNAs and progression of oocyte maturation. Pum1 was shown to bind to *Mad2* (also known as *Mad2l1*) and cyclin B1 mRNAs, assemble highly clustered aggregates, and surround *Mad2* and cyclin B1 RNA granules in mouse oocytes. These Pum1 aggregates were dissolved prior to the translational activation of target mRNAs, possibly through phosphorylation. Stabilization of Pum1 aggregates prevented the translational activation of target mRNAs and progression of oocyte maturation. Together, our results provide an aggregation-dissolution model for the temporal and spatial control of translation.

KEY WORDS: Pumilio 1, Vertebrate, mRNA localization, Oocyte, Meiosis, Translational control

INTRODUCTION

Diverse biological processes, including meiosis, embryonic development and neuronal plasticity, are promoted by translational activation of dormant mRNAs at appropriate timings and places (Buxbaum et al., 2015; Martin and Ephrussi, 2009; Mendez and Richter, 2001; Mili and Macara, 2009). This temporal control of translation has been most extensively studied in oocyte meiosis. Fully grown vertebrate oocytes are arrested at prophase I of meiosis and accumulate thousands of translationally repressed mRNAs in the cytoplasm (Kotani et al., 2017; Masui and Clarke, 1979; Winata and Korzh, 2018). In response to specific cues, such as hormones, oocytes resume meiosis and are arrested again at metaphase II. This process is termed oocyte maturation and is necessary for oocytes to acquire fertility. For proper progression of oocyte maturation, hundreds of dormant mRNAs are translationally activated in periods specific to distinct mRNAs (Chen et al., 2011; Luong et al., 2020), which are generally categorized as early meiosis I, late meiosis I and meiosis II. Of these, cyclin B1 mRNA, which encodes the regulatory subunit of maturation/M-phase-promoting factor (MPF), is translated in the early period of meiosis I, and the newly synthesized cyclin B1 proteins in this period are a prerequisite for the progression of meiosis (Davydenko et al., 2013; Kondo et al., 2001; Kotani and Yamashita, 2002; Ledan et al., 2001; Polanski et al., 1998).

Translational activation of the dormant mRNAs, including cyclin B1, has been shown to be directed by the cytoplasmic polyadenylation of mRNAs, which is mediated by the cytoplasmic polyadenylation element (CPE) in their 3′ UTR (McGrew et al., 1989; Sheets et al., 1994). The CPE-binding protein 1 (CPEB1) functions in both repression and direction of the cytoplasmic polyadenylation (Barkoff et al., 2000; de Moor and Richter, 1999; Gebauer et al., 1994; Tay et al., 2000). Although many dormant mRNAs contain CPEs, they are translated in different periods during oocyte maturation, indicating that there must be additional mechanisms to determine the timings of translational activation of distinct mRNAs. However, the molecular and cellular mechanisms by which translational timings of hundreds of mRNAs are coordinated remain unclear.

Pumilio 1 (Pum1) is a sequence-specific RNA-binding protein that belongs to the Pumilio and Fem-3 mRNA-binding factor (PUF) family, which is highly conserved in eukaryotes from yeast to human (Spassov and Jurecic, 2003; Wickens et al., 2002). Pum was identified in *Drosophila* as a protein that is essential for posterior patterning of embryos (Lehmann and Nüsslein-volhard, 1987) and it was shown to repress the translation of target mRNAs in a spatially and temporally regulated manner (Asaoka-Taguchi et al., 1999; Murata and Wharton, 1995). In *Xenopus*, zebrafish and mouse oocytes, Pum1 has been shown to bind to cyclin B1 mRNA and determine the timing of translational activation of cyclin B1 mRNA during oocyte maturation (Kotani et al., 2013; Nakahata et al., 2003; Ota et al., 2011a; Piqué et al., 2008). Pum1-knockout mice are viable but defective in spermatogenesis (Chen et al., 2012) and oogenesis (Mak et al., 2016). Pum1-deficient mice also showed neuronal degeneration in the brain, which is caused by an increase in ataxin 1 protein (Gennarino et al., 2015). In the mouse testis and brain, Pum1 was shown to target more than 1000 mRNAs (Chen et al., 2012; Zhang et al., 2017). The amount of protein synthesized from these Pum1-target mRNAs, but not the amount of mRNA, was increased in Pum1-deficient mice, indicating that Pum1 represses the translation of target mRNAs (Chen et al., 2012; Zhang et al., 2017). Despite the importance of Pum function in diverse systems, how Pum regulates the translation of target mRNAs remains to be elucidated.

In addition to sequence-specific RNA-binding proteins, we previously demonstrated that formation and disassembly of cyclin B1 RNA granules determine the timing of translational activation of

[1]Biosystems Science Course, Graduate School of Life Science, Hokkaido University, Sapporo 060-0810, Japan. [2]Development and Stem Cells Program and Department of Anatomy and Developmental Biology, Monash Biomedicine Discovery Institute, Monash University, Melbourne, Victoria 3800, Australia. [3]Department of Biological Sciences, Faculty of Science, Hokkaido University, Sapporo 060-0810, Japan.
*These authors contributed equally to this work

‡Author for correspondence (tkotani@sci.hokudai.ac.jp)

N.T., 0000-0003-2533-1335; Y.T., 0000-0003-4710-3448; S.K., 0000-0002-3751-246X; K.S., 0000-0002-8514-4016; A.S., 0000-0003-2170-9548; W.S.Y., 0000-0002-9968-3571; T.K., 0000-0003-1930-6635

Handling Editor: Maria Carmo-Fonseca
Received 19 May 2020; Accepted 22 October 2020

Journal of Cell Science (2020) 133, jcs249128. doi:10.1242/jcs.249128

mRNA; the granular structures of cyclin B1 mRNA formed in immature germinal vesicle (GV)-stage oocytes were disassembled at the same time as translational activation of mRNA, and stabilization and dissociation of these granules prevented and accelerated the mRNA translation, respectively (Kotani et al., 2013). Binding of Pum1 was shown to be required for the RNA granule formation, implying that Pum1 regulates the translational timing of target mRNAs through formation and disassembly of granules (Kotani et al., 2013).

P granules are cytoplasmic granules that consist of mRNAs and RNA-binding proteins, and have been shown to behave as liquid droplets with a spherical shape in *C. elegance* embryos (Brangwynne et al., 2009). In addition, several RNA-binding proteins that are assembled into stress granules have been shown to produce liquid droplets *in vitro* and in cultured cells (Lin et al., 2015; Molliex et al., 2015). Although phase changes in these liquid droplets into solid-like assemblies have been linked to degenerative diseases (Li et al., 2013; Weber and Brangwynne, 2012), more recent studies have demonstrated the assembly of solid-like substructures within stress granules (Jain et al., 2016; Shiina, 2019), suggesting physiological roles of the solid-like assemblies.

In this study, we identified *Mad2* mRNA as one of the Pum1-target mRNAs in mouse oocytes and found that *Mad2* and cyclin B1 mRNAs were distributed as distinct granules in the cytoplasm. Interestingly, Pum1 was assembled into aggregates exhibiting highly clustered structures, and these aggregates surrounded *Mad2* and cyclin B1 RNA granules. The Pum1 aggregates dissolved shortly after resumption of meiosis, possibly because of phosphorylation, resulting in translational activation of *Mad2* and cyclin B1 mRNAs in early meiosis I. These results provide an aggregation–dissolution model for temporal and spatial control of mRNA translation. Since Pum1 aggregates resembled solid-like assemblies, the results suggest the physiological importance of phase changes of proteins during RNA regulation.

RESULTS

Expression of Mad2 is translationally regulated during mouse oocyte maturation

Mad2 has been shown to function as a component of spindle assembly checkpoint proteins to ensure accurate segregation of chromosomes in meiosis I of mouse oocytes (Homer et al., 2005). However, how Mad2 is accumulated in oocytes remains unknown. To clarify the mechanism of Mad2 accumulation in meiosis I, we first analyzed the expression of *Mad2* mRNA in mouse oocytes. Using purified RNAs from ovaries, we determined that there were two splicing variants of *Mad2* mRNA by RT-PCR analysis (Fig. 1A). RT-PCR and quantitative PCR analyses of oocytes isolated from ovaries showed that the short version of *Mad2* mRNA was dominant in oocytes (Fig. 1A,B). In addition, *in situ* hybridization analysis of ovary sections with the tyramide signal amplification (TSA) system detected the expression of short, but not long, *Mad2* mRNA in oocytes (Fig. 1C). Fluorescence *in situ* hybridization (FISH) analysis showed that short *Mad2* mRNA was distributed in the oocyte cytoplasm where it was present as RNA granules (Fig. 1D). In contrast, long *Mad2* mRNA was not detected by FISH analysis (Fig. S1A). These results suggest that short *Mad2* mRNA is crucial for the synthesis of Mad2 protein in oocytes.

We then analyzed the expression of Mad2 protein in oocytes. Immunoblot analysis showed that the amount of Mad2, as well as that of cyclin B1, increased after resumption of meiosis (Fig. 1E). Consistent with this, a poly(A) test (PAT) assay showed that the poly(A) tails of *Mad2* mRNA were elongated 4 h after resumption of meiosis, as is the case for cyclin B1 (Fig. 1F). Inhibition of protein synthesis with puromycin prevented the accumulation of Mad2 in oocytes even when meiosis had resumed (Fig. S1B). To rule out a possibility that Mad2 protein becomes stabilized after resumption of meiosis, we analyzed the stability of Mad2 by expressing GFP–Mad2 followed by puromycin treatment. The rate of destruction of GFP–Mad2 in immature oocytes was similar to that in mature oocytes (Fig. S1C), indicating that the stability of Mad2 is not changed. Taken together, these results indicate that Mad2 protein accumulates during the early period of oocyte maturation because of the translational activation of dormant mRNA stored in oocytes.

Mad2 mRNA is a Pum1-target mRNA and forms granules that are distinct from cyclin B1 RNA granules

We then assessed the mechanism by which the translation of *Mad2* mRNA is temporally regulated. Since *Mad2* mRNA was translated in a period similar to that of cyclin B1 mRNA and contains several putative pumilio-binding elements (PBEs) in its 3′UTR (Fig. S2A), we investigated whether Pum1 binds to *Mad2* mRNA by using an immunoprecipitation assay followed by RT-PCR. *Mad2* and cyclin B1 mRNAs, but not α-tubulin and β-actin mRNAs, were detected in precipitations with an anti-Pum1 antibody, while neither of them was detected in precipitations with control IgG (Fig. 2A), indicating that Pum1 targets *Mad2* mRNA as well as cyclin B1 mRNA. From these results, we speculated that both mRNAs were assembled into the same granules. However, double FISH analysis showed that the two mRNAs formed distinct granules (Fig. 2B). The granules containing *Mad2* mRNA rarely overlapped with those containing cyclin B1 mRNA (0.18%, n=2748). Formation of distinct granules of *Mad2* and cyclin B1 mRNAs resembles formation of *Map2*, CaMKIIα and β-actin RNA granules in neurons, in which distinct mRNAs were assembled into different granules (Mikl et al., 2011).

Time course analysis showed that the number of *Mad2* RNA granules was decreased at 4 h (prometaphase I) and that the granules had almost completely disappeared at 18 h (metaphase II) after resumption of meiosis, which is consistent with the changes in cyclin B1 RNA granules (Fig. 2C,D) (Kotani et al., 2013). The amount of *Mad2* mRNA was not changed in oocytes at 18 h after resumption of meiosis (Fig. S2B), indicating that the decrease in the number of *Mad2* RNA granules is caused by granule disassembly. These results suggest that translation of *Mad2* mRNA is temporally regulated through formation and disassembly of RNA granules, similar to the cytoplasmic regulation of cyclin B1 mRNA (Kotani et al., 2013).

Pum1 forms aggregates that surround target mRNAs

To further assess the mechanism by which translation of *Mad2* and cyclin B1 mRNAs is temporally and spatially regulated by Pum1, we analyzed the distribution of Pum1 in the oocyte cytoplasm. Immunofluorescence analysis showed that Pum1 was non-uniformly distributed in the cytoplasm of immature oocytes and appeared to form aggregates in highly clustered structures (Fig. 3A). This signal was specific to Pum1 since no signal was detected when the antibody was absorbed with N-terminus region of Pum1 (amino acids 1–399) (Fig. S2C), which includes the region recognized by the antibody (amino acids 225–275). Simultaneous detection of Pum1 protein and cyclin B1 and *Mad2* mRNAs showed that clusters of Pum1 aggregates covered cyclin B1 and *Mad2* RNA granules (Fig. 3B,C). In most cases, Pum1 aggregates surrounded and partially overlapped with cyclin B1 and *Mad2* RNA granules at the periphery (Fig. 3C; 95.1%, n=268 for cyclin B1; 98.4%, n=124 for *Mad2*), while in remaining cases Pum1 aggregates were localized at

Journal of Cell Science (2020) 133, jcs249128. doi:10.1242/jcs.249128

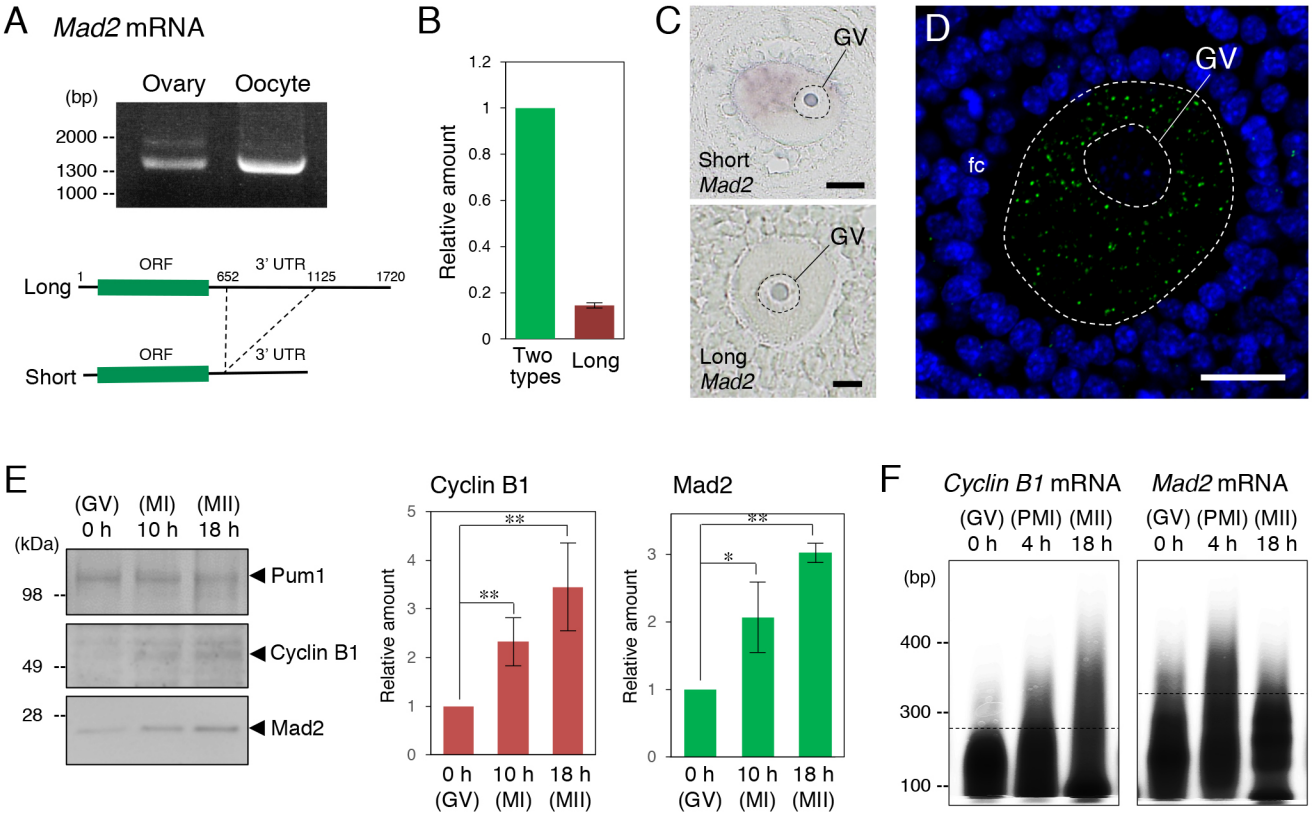

Fig. 1. Expression and translational regulation of *Mad2* mRNA in mouse oocytes. (A) Top, RT-PCR amplification for *Mad2* mRNA in the mouse ovary and oocyte. Similar results were obtained from three independent experiments. Bottom, schematic views of long and short *Mad2* mRNAs (GenBank number: BC089012.1 and NM_001355624.1, respectively). (B) Quantitative PCR for the two types of *Mad2* mRNA and for long *Mad2* mRNA in oocytes (mean±s.d.; n=3). (C) Detection of *Mad2* mRNA in oocytes by *in situ* hybridization with the TSA system. Similar results were obtained from three independent experiments. (D) FISH analysis of *Mad2* mRNA (green). DNA is shown in blue. Similar results were obtained from three independent experiments. (E) Left, immunoblotting of Pum1, cyclin B1 and Mad2 in oocytes at 0, 10 and 18 h after resumption of meiosis. Right, quantitative analysis (mean±s.d.; n=3). *P<0.05, **P<0.01 (unpaired t-test). (F) Poly(A) tail analysis of cyclin B1 and *Mad2* mRNAs in oocytes at 0, 4 and 18 h after resumption of meiosis. Similar results were obtained from three independent experiments. GV, germinal vesicle; fc, follicle cells. Scale bars: 20 µm.

the center of granules in addition to the periphery (Fig. 3C; 4.9% for cyclin B1; 1.6% for *Mad2*). These distribution patterns were specific to *Mad2* and cyclin B1 mRNAs since (1) the average distance between randomly distributed dots and Pum1 aggregates was 1.8-fold longer than the experimental distance between the center of RNA granules and Pum1 aggregates (P<0.001) (Monte Carlo simulation; 100 permutations) and (2) α-tubulin mRNA was not surrounded by Pum1 and instead it was uniformly distributed in the cytoplasm (Fig. S2D).

To assess the molecular mechanisms of Pum1 aggregation, we then examined the distribution of GFP–Pum1 and mutant forms of Pum1 by injecting mRNA into mouse oocytes. GFP-Pum1 was distributed in a way similar to that of endogenous Pum1, i.e. it appeared to form highly clustered aggregates (Fig. 3D,E) and surrounded cyclin B1 and *Mad2* RNA granules (Fig. S2E). Pum1 contains a glutamine/asparagine (Q/N)-rich domain (Fig. 3F), also identified as a prion-like domain (Fig. S2F; Lancaster et al., 2014), which is thought to promote highly ordered aggregation of proteins (Lancaster et al., 2014; Salazar et al., 2010). GFP–Pum1 that lacks the Q/N-rich domain (GFP–Pum1ΔQN) (Fig. 3F) was distributed uniformly throughout the oocyte cytoplasm (Fig. 3D). Taken together, these results indicate that Pum1 assembles into highly clustered aggregates and that this is mediated by the Q/N-rich domain, and that these aggregates cover target mRNAs.

We then analyzed the distribution of Pum1 lacking the N-terminus (GFP–Pum1ΔN) or lacking the C-terminus, which contains the PUF domain, which is responsible for binding to target mRNAs (Zhang et al., 1997) (GFP–Pum1ΔC; Fig. 3F). GFP–Pum1ΔN formed aggregates similar to those of GFP–Pum1 (Fig. S2G, and see Fig. 6A). In contrast, GFP–Pum1ΔC formed aggregates larger than those of GFP–Pum1 (Fig. S2G, and see Fig. 6A), indicating that the C-terminal PUF domain is involved in regulating the size of aggregates.

Pum1 shows insoluble and immobile properties in immature oocytes

We then examined the properties of endogenous Pum1 by ultracentrifugation. Since we were unable to obtain appropriate amounts of materials by using mouse oocytes, we used zebrafish oocytes for this analysis. Zebrafish Pum1 has been shown to target cyclin B1 mRNA (Kotani et al., 2013) and it contains the Q/N-rich domain also identified as a prion-like domain (Fig. S2F). Ultracentrifugation analysis showed that most of the endogenous Pum1 (64.8±3.4%, mean±s.d., n=3) was concentrated in an insoluble fraction in immature oocytes (Fig. 4A), supporting the results of the immunofluorescence showing that endogenous Pum1 forms aggregates (Fig. 3).

We next examined the properties of GFP–Pum1 in mouse oocytes by fluorescence recovery after photobleaching (FRAP) analysis. As

Journal of Cell Science (2020) 133, jcs249128. doi:10.1242/jcs.249128

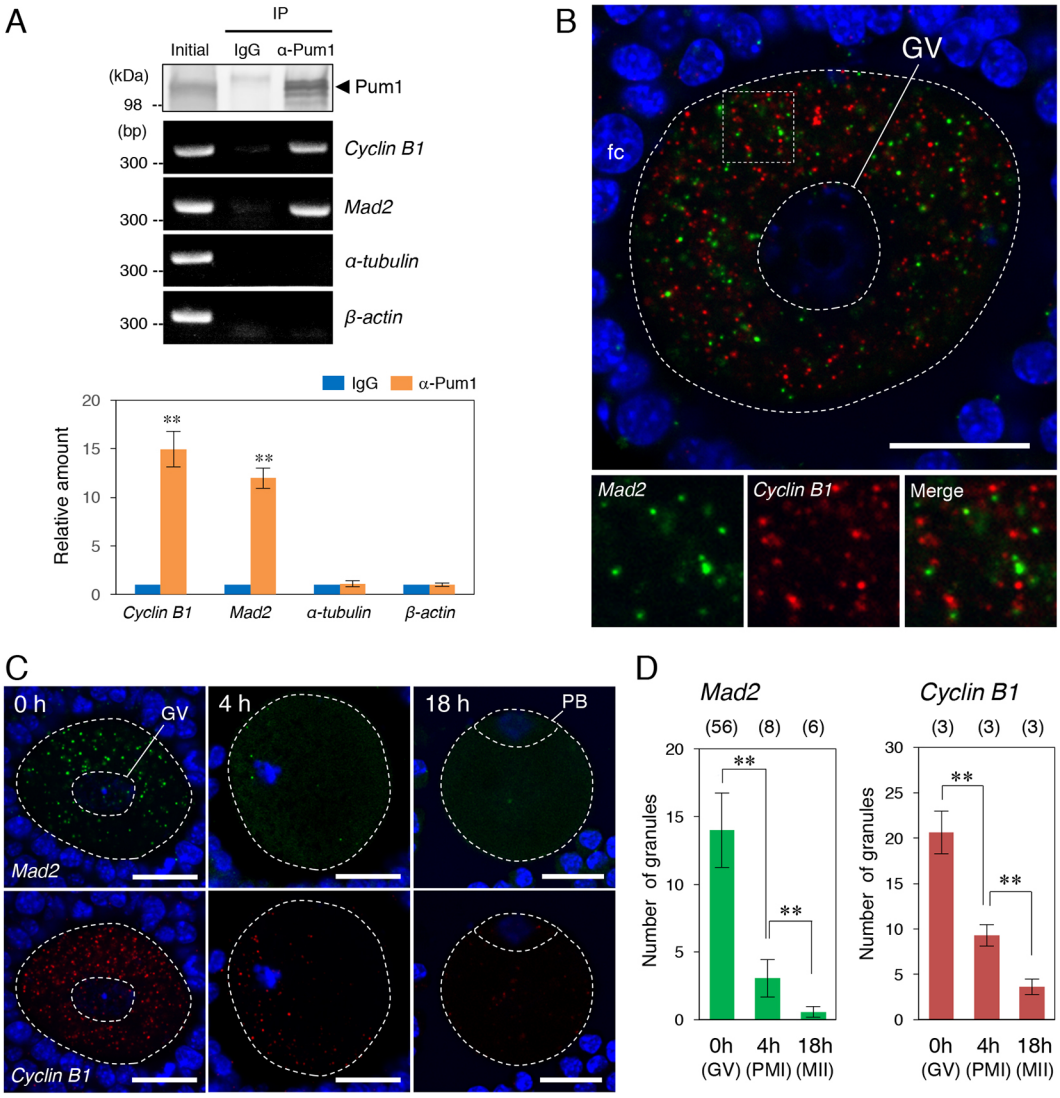

Fig. 2. Interaction with Pum1 and cytoplasmic regulation of *Mad2* mRNA in mouse oocytes. (A) Top, immunoblotting of Pum1 and semi-quantitative RT-PCR for cyclin B1, *Mad2*, α-tubulin and β-actin transcripts of ovary extracts before immunoprecipitation (IP) (Initial) and after IP with goat IgG (IgG) or anti-Pum1 goat antibody (α-Pum1). Bottom, quantitative analysis (mean±s.d.; n=3). **P<0.01 (unpaired t-test). (B) FISH analysis of *Mad2* (green) and cyclin B1 (red) mRNAs in a mouse oocyte. DNA is shown in blue. Enlarged views of the boxed region are shown underneath. Similar results were obtained from three independent experiments. (C) FISH analysis of oocytes at 0, 4 and 18 h after resumption of meiosis. (D) The numbers of RNA granules per 100 μm^2 in individual oocytes at 0, 4, and 18 h were counted (mean±s.d.). The numbers in parentheses indicate the total numbers of oocytes analyzed. **P<0.01 (unpaired t-test). GV, germinal vesicle; fc, follicle cells; PB, polar body. Dashed lines outline edge of indicated regions or oocyte. Scale bars: 20 μm.

a control, GFP–Pum1ΔQN was analyzed. After photobleaching, the fluorescence of GFP–Pum1 and GFP–Pum1ΔQN gradually recovered (Fig. 4B). The fluorescence recovery curves were fitted to a double exponential association model (Fig. S3). The halftime of recovery ($t_{1/2}$) of the first fraction of GFP–Pum1 was rapid, while that of the second fraction of GFP–Pum1 was slow (Fig. 4C, left), suggesting that a proportion of Pum1 is in large complexes. Moreover, a critical finding was that a significant fraction of GFP–Pum1 (40.7±8.6%, mean±s.d., n=12) showed immobility (not recovering after photobleaching), while only a small fraction of GFP–Pum1ΔQN (13.6±5.5%, n=14) was static (Fig. 4B,C, right). Thereby, the Q/N-rich region promotes the assembly of Pum1 into highly ordered aggregates in an immobile state. To analyze the details of Pum1 recovery after photobleaching, we observed changes in GFP–Pum1 in aggregates using a high-resolution microscope. The intensity of GFP–Pum1 in aggregates recovered slowly and only partially (Fig. 4D), supporting the notion that Pum1 aggregates exhibit an immobile property.

We further analyzed the properties of Pum1 by permeabilizing oocytes with digitonin. A recent study demonstrated that liquid-like droplets of RNA-binding proteins rapidly shrunk and dissolved within 2 to 3 min after this treatment, while stable assemblies of RNA-binding proteins that exhibit solid-like properties were maintained in cultured cells (Shiina, 2019). After permeabilization with digitonin, GFP rapidly diffused out of the oocytes (Fig. 4E,F). In contrast, the structure and intensity of GFP–Pum1 aggregates persisted after permeabilization (Fig. 4E,F). Collectively, the immunofluorescence, ultracentrifugation, FRAP and permeabilization analyses suggest that Pum1 assembles into aggregates in a solid-like state in immature oocytes. The study by Shiina (Shiina, 2019) demonstrated that GFP–Pum1 forms solid-like substructures of RNA granules in cultured cells, which is consistent with our results in oocytes.

Journal of Cell Science (2020) 133, jcs249128. doi:10.1242/jcs.249128

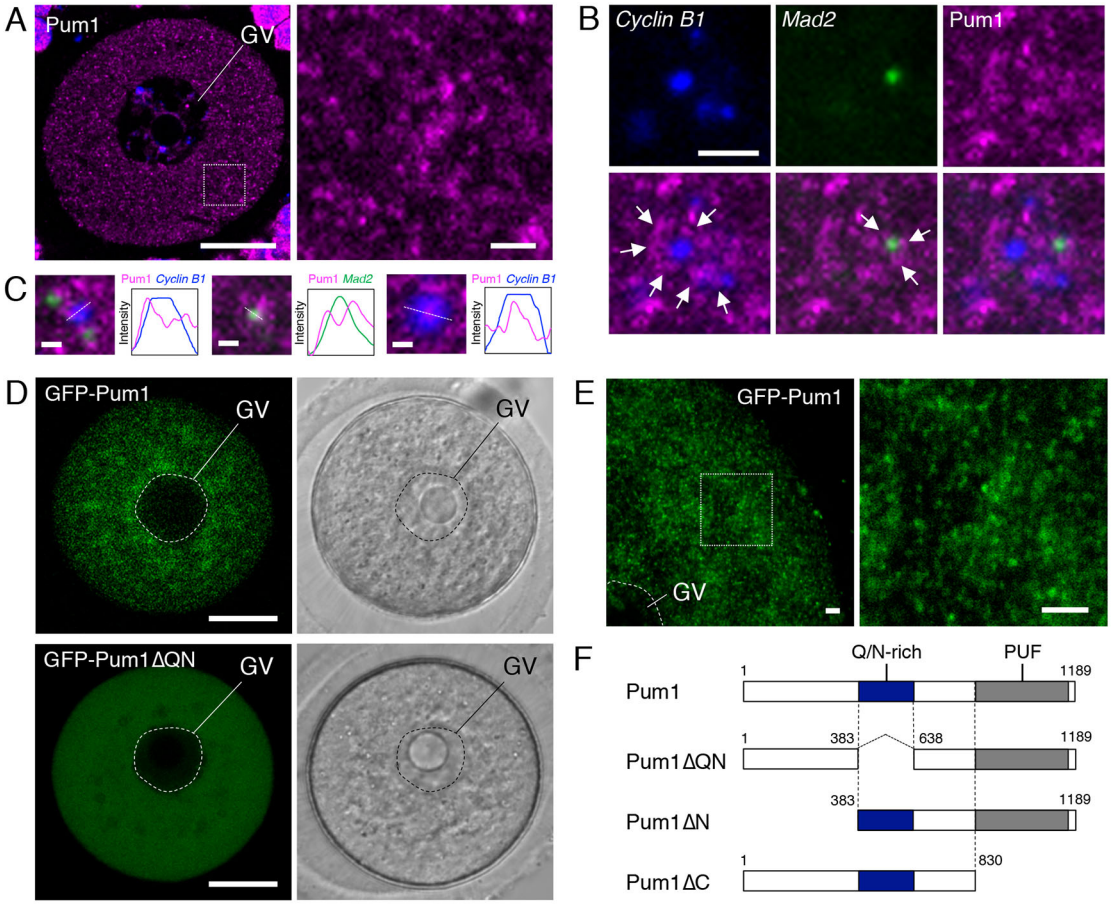

Fig. 3. Formation of Pum1 aggregates that surround cyclin B1 and *Mad2* RNA granules. (A) Left, immunofluorescence of Pum1 (magenta) in immature oocytes. DNA is shown in blue. Right, an enlarged view of the boxed region. Similar results were obtained from three independent experiments. (B) FISH analysis of cyclin B1 (blue) and *Mad2* (green) mRNAs and immunostaining of Pum1 (magenta) in immature oocytes. Arrows indicate Pum1 aggregates surrounding cyclin B1 and *Mad2* RNA granules. Similar results were obtained from three independent experiments. (C) Representative images of the distribution of Pum1 (magenta) and cyclin B1 (blue) and *Mad2* (green) mRNAs. Line graphs display intensity profiles along the dotted lines. (D) Distributions of GFP–Pum1 (top) and GFP–Pum1ΔQN (bottom). Bright field images are shown on the right. (E) Left, a high-resolution image of GFP–Pum1. Right, an enlarged view of the boxed region. Similar results were obtained from six independent experiments. (F) Schematic diagrams of Pum1, Pum1ΔQN, Pum1ΔN and Pum1ΔC. GV, germinal vesicle. Dashed lines outline edge of indicated regions or oocyte. Scale bars: 20 µm (A, left; D), 2 µm (A, right; B,E), 0.5 µm (C).

Pum1 aggregates are dissolved prior to translational activation of target mRNAs

We next examined whether the distribution and properties of Pum1 changed during oocyte maturation. Time course analysis of GFP–Pum1 showed that the Pum1 aggregates disappeared after resumption of meiosis (Fig. 5A). Most of the aggregates of GFP–Pum1 had disappeared 4 h after resumption of meiosis, at which time poly(A) tails of *Mad2* and cyclin B1 mRNA were elongated (Fig. 1F) and the granules of both RNAs had disappeared (Fig. 2C), suggesting a link between translational activation of target mRNAs and Pum1 dissolution. Consistent with these observations, the ultracentrifugation assay showed that a large proportion of endogenous Pum1 was soluble (69.0±4.4%, n=3) in mature oocytes, compared with the proportion in the soluble fraction in immature oocytes (35.2±3.4%, n=3) (Fig. 4A). In contrast, the Golgi matrix protein GM130 (also known as GOLGA2) remained insoluble in mature oocytes (Fig. 4A). FRAP analysis in mouse oocytes indicated that the $t_{1/2}$ of GFP–Pum1 was not significantly different between immature and mature oocytes (Fig. 5B,C, left). In contrast, the percentage of GFP–Pum1 in the immobile fractions was significantly reduced in mature oocytes (18.8±6.8%, n=6) compared with that in immature oocytes (40.7±8.6%, n=12) (Fig. 5B,C, right). Taken together, these results indicate that Pum1 aggregates dissolve during oocyte maturation and suggest that there is a relationship between changes in the property of Pum1 and temporal regulation of target mRNA translation.

Stabilization of Pum1 aggregates prevents the translation of target mRNAs

We next assessed whether the change in the aggregation status of Pum1 was involved in the translational regulation of target mRNAs. Through observing the distributions of truncated forms of Pum1 after resumption of meiosis, we found that the large aggregates of GFP–Pum1ΔC were stable and persisted until 18 h (Fig. 6A). In contrast, GFP–Pum1ΔQN no longer formed aggregates (Fig. S4A), and the aggregates of GFP–Pum1ΔN dissociated within 4 h (Fig. S4B; Fig. 6A). Consistent with the observations after resumption of meiosis, GFP–Pum1, GFP–Pum1ΔQN and GFP–Pum1ΔN did not affect the progression of oocyte maturation, while GFP–Pum1ΔC prevented polar body extrusion (Fig. 6A,B). Temporal synthesis of proteins is required for proper spindle formation in meiosis I (Davydenko et al., 2013; Kotani and Yamashita, 2002; Polanski et al., 1998; Susor et al., 2015). In oocytes expressing GFP–Pum1ΔC, meiosis I spindles were defective, while correct meiosis II

Journal of Cell Science (2020) 133, jcs249128. doi:10.1242/jcs.249128

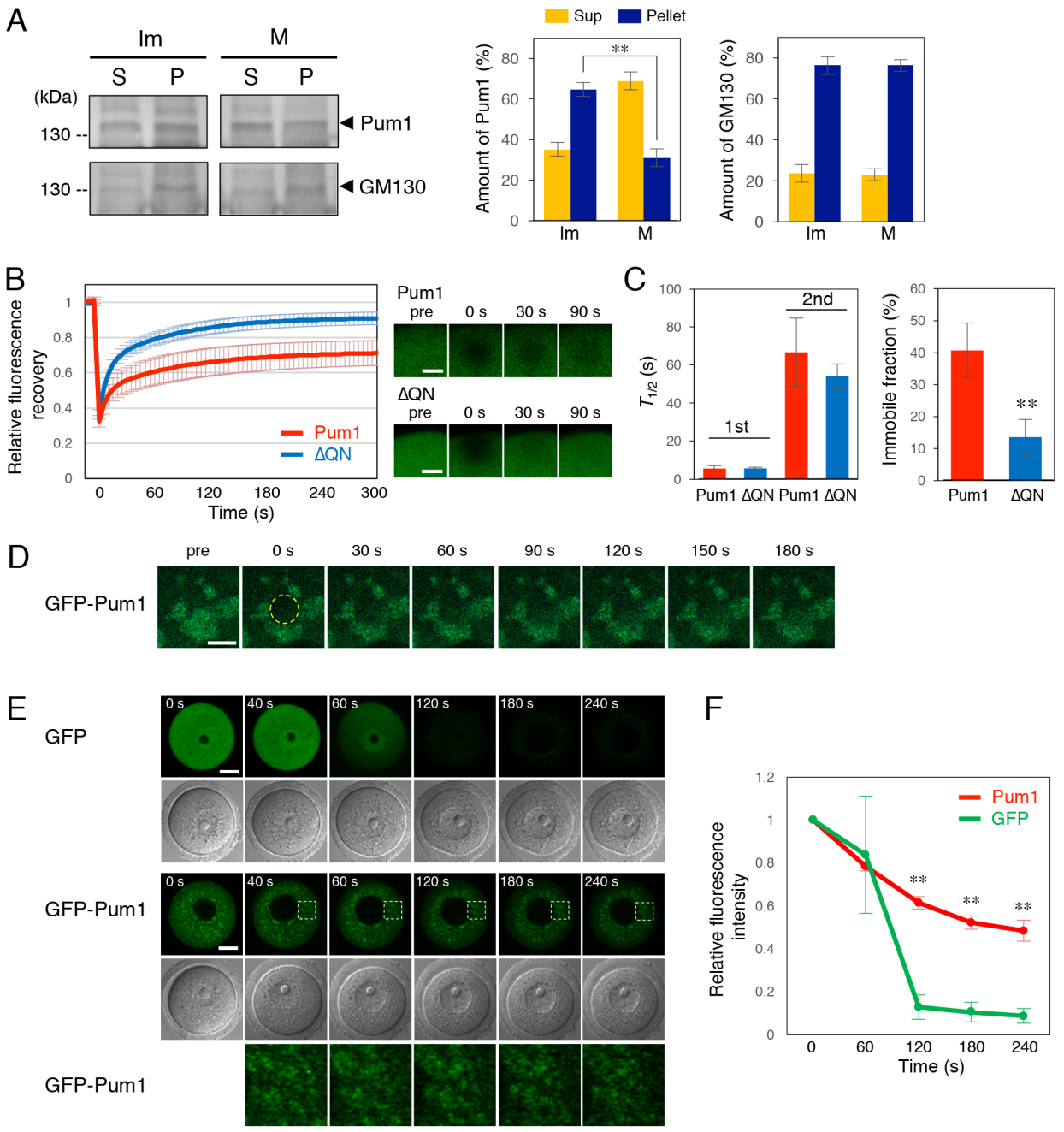

Fig. 4. Insoluble and immobile properties of Pum1 in immature oocytes. (A) Left, ultracentrifugation analysis of Pum1. Immature (Im) and mature (M) zebrafish oocytes were centrifuged, and the supernatant (S) and pellet (P) equivalent to one oocyte were analyzed by immunoblotting. GM130 is a Golgi matrix protein. Right, quantitative analysis of Pum1 and GM130 (means±s.d.; n=3). **P<0.01 (unpaired t-test). (B) FRAP analysis of GFP–Pum1 (Pum1) and GFP–Pum1ΔQN (ΔQN) in immature mouse oocytes. Fluorescence recovery curves for GFP–Pum1 (n=12) and GFP–Pum1ΔQN (n=14) are shown (mean±s.d.). (C) Values of $t_{1/2}$ (left) and percentages of GFP–Pum1 and GFP–Pum1ΔQN present in the immobile fraction (right). **P<0.01 (unpaired t-test). (D) Time course of GFP–Pum1 after photobleaching (yellow circle) obtained using a high-resolution microscope. (E) Time course of GFP and GFP–Pum1 after permeabilization with digitonin. Similar results were obtained in 11 oocytes from two independent experiments. (F) Quantitative analysis of fluorescence intensity in E (mean±s.d.; n=3). **P<0.01 (unpaired t-test relative to GFP). Scale bars: 10 µm (B), 5 µm (D), 20 µm (E).

spindles were formed in oocytes expressing GFP at 18 h after resumption of meiosis (Fig. 6C).

We found that RNA granules of *Mad2* and cyclin B1 disappeared in oocytes expressing GFP and GFP–Pum1, GFP–Pum1ΔQN and GFP–Pum1ΔN at 4 h after resumption of meiosis (Fig. 6D,E), as in the case of non-injected oocytes (Fig. 2C,D). In contrast, both RNA granules were maintained in oocytes expressing GFP–Pum1ΔC, although the number of cyclin B1 RNA granules was slightly decreased (Fig. 6D,E). Aggregates of GFP–Pum1ΔC, but not GFP alone, surrounded cyclin B1 RNA granules (Fig. S4C). The amounts of GFP–Pum1 and mutant forms of Pum1 were 1.6–1.8-fold larger than those of endogenous Pum1 (Fig. S4D). Synthesis of Mad2 and cyclin B1 was attenuated in oocytes expressing GFP–Pum1ΔC, while the amounts of both proteins were not changed in oocytes expressing GFP and GFP–Pum1, Pum1ΔQN and Pum1ΔN (Fig. 6F; Fig. S5A). These results suggest that insoluble

Journal of Cell Science (2020) 133, jcs249128. doi:10.1242/jcs.249128

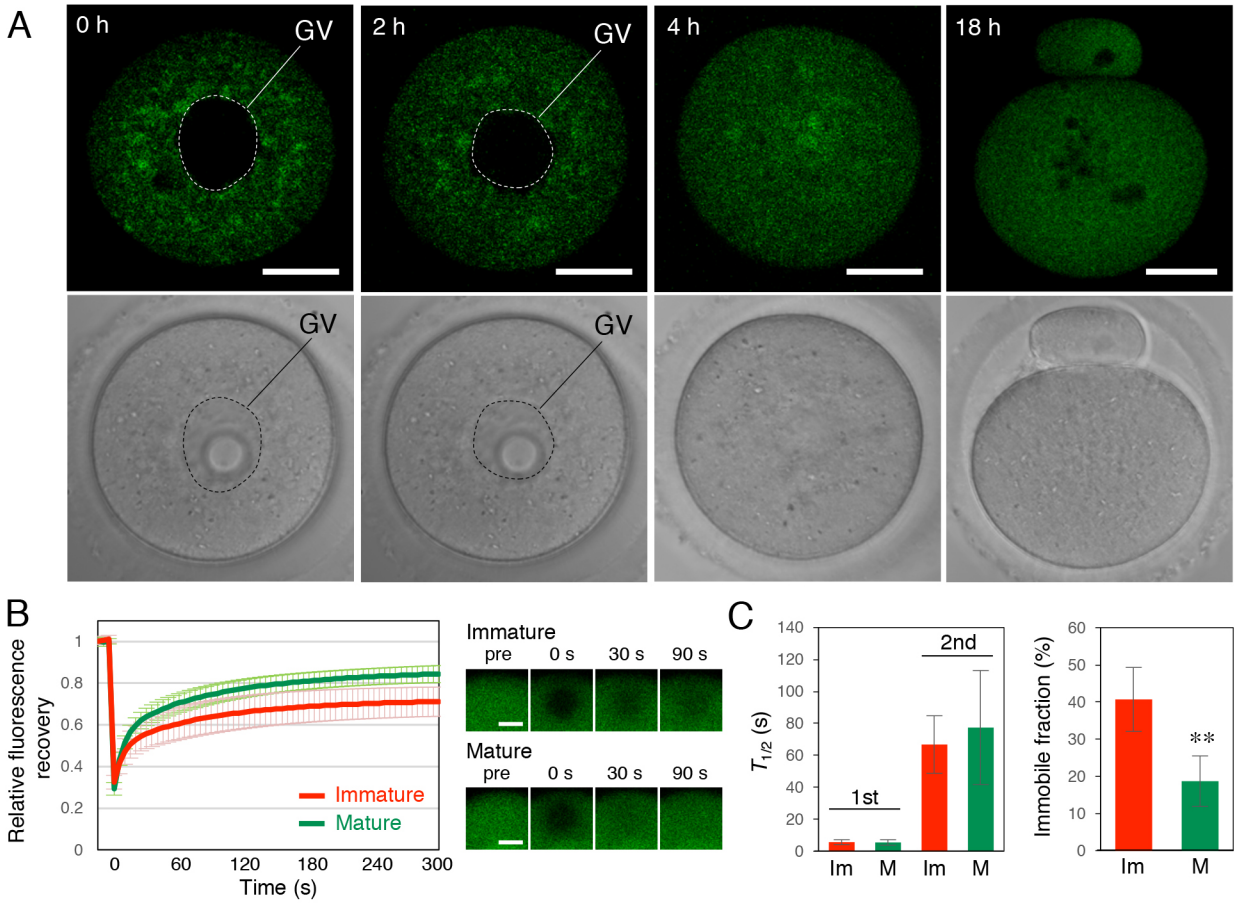

Fig. 5. Insoluble and immobile properties of Pum1 are changed during oocyte maturation. (A) Time course of GFP–Pum1 at 0, 2, 4 and 18 h after resumption of meiosis. Similar results were obtained from six independent experiments. Dashed lines outline edge of germinal vesicle (GV). (B) FRAP analysis of GFP–Pum1 in immature and mature mouse oocytes. Fluorescence recovery curves in immature (n=12) and mature (n=6) oocytes are shown (mean±s.d.). (C) Values of half time of recovery ($t_{1/2}$) of the first (1st) and second (2nd) fractions of GFP–Pum1 (left) and percentage of GFP–Pum1 (right) present in immobile fractions for immature (Im) and mature (M) oocytes. **P<0.01 (unpaired t-test). Scale bars: 20 µm (A), 10 µm (B).

GFP-Pum1ΔC inhibited translational activation of Pum1-target mRNAs by stabilizing Pum1 aggregates and RNA granules, resulting in failure in spindle formation and polar body extrusion.

Cyclin B1 synthesis after resumption of meiosis has been shown to promote bipolar spindle formation in meiosis I via activating MPF in meiosis I (Polanski et al., 1998). At 9 h after resumption of meiosis, bipolar structures of meiosis I spindles were observed in oocytes expressing GFP (94% of oocytes, n=17) as in the case of non-injected oocytes (89% of oocytes, n=9), while meiosis I spindles were still in round shapes without poles in oocytes expressing GFP–Pum1ΔC (60% of oocytes, n=15) (Fig. 6G), which is consistent with the attenuation of cyclin B1 synthesis (Fig. 6F). Injection of cyclin B1 mRNA carrying the SV40 3′UTR, which lacks PBE, at 1 h after resumption of meiosis completely rescued the formation of bipolar spindles (100% of oocytes, n=8) (Fig. 6G). The results indicate that the inhibition of protein synthesis by expression of GFP–Pum1ΔC is indeed a cause of the abnormal progression of meiosis. Since Pum1 targets thousands of mRNAs in the testis and brain (Chen et al., 2012; Zhang et al., 2017), syntheses of many proteins responsible for correct spindle formation would be attenuated in oocytes expressing GFP–Pum1ΔC.

We then examined the effects of Pum1 inhibition on the progression of oocyte maturation by injecting the anti-Pum1 antibody. To effectively analyze the effect of the anti-Pum1 antibody, we incubated oocytes with 1 µM milrinone, which partially prevents resumption of meiosis. Under this condition, 50–100% of the oocytes underwent germinal vesicle breakdown (GVBD) (Fig. 7A,B) in a manner dependent on protein synthesis since puromycin treatment prevented GVBD (Fig. 7A). Injection of the anti-Pum1 antibody, but not control IgG, prevented GVBD, dissolution of GFP–Pum1 aggregates, and synthesis of cyclin B1 and Mad2 (Fig. 7B–D; Fig. S5B). The injected anti-Pum1 antibody was distributed within the cytoplasm in a similar manner to that of endogenous Pum1 (Fig. 7E). These results strongly suggest that the anti-Pum1 antibody inhibited the dissolution of endogenous Pum1 aggregates and thereby prevented the translational activation of Pum1-target mRNAs.

Pum1 phosphorylation is linked with the dissolution of aggregates

We finally assessed the mechanism by which Pum1 aggregates are dissolved. As observed in *Xenopus* and zebrafish (Ota et al., 2011a; Saitoh et al., 2018), the electrophoretic mobility of Pum1 was reduced in mature mouse oocytes (Fig. 8A, left). This reduction was recovered upon phosphatase treatment (Fig. 8A, right), indicating that Pum1 is phosphorylated during mouse oocyte maturation. Treatment of immature oocytes with okadaic acid (OA), a protein phosphatase 1 and 2A (PP1 and PP2A) inhibitor (Bialojan and Takai, 1988), induced Pum1 phosphorylation and rapid dissolution of Pum1 aggregates (Fig. 8B–D). These results suggest that kinases

Journal of Cell Science (2020) 133, jcs249128. doi:10.1242/jcs.249128

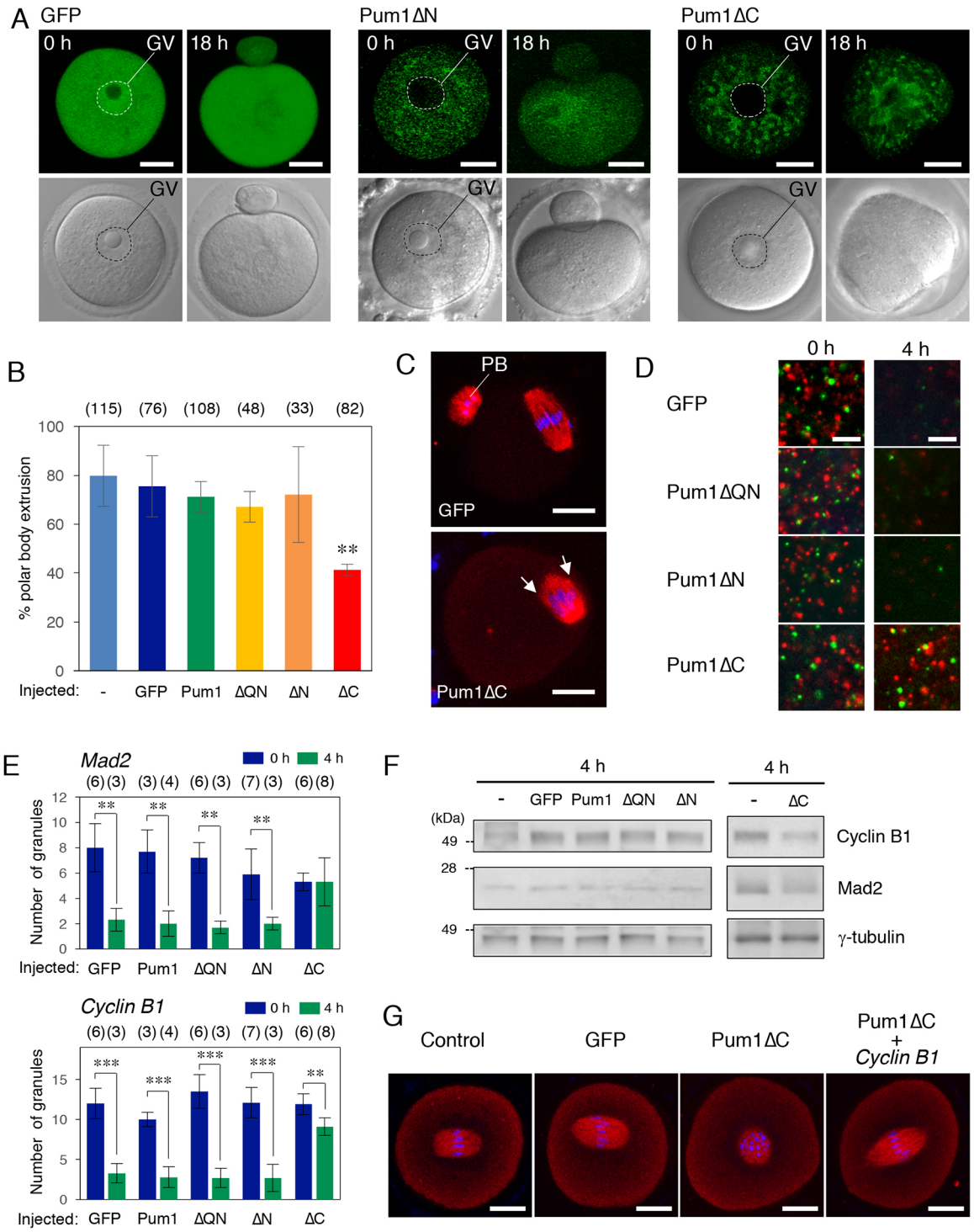

Fig. 6. Stabilization of Pum1 aggregates through expression of Pum1ΔC prevents the translation of target mRNA. (A) Distributions of GFP, GFP-Pum1ΔN and GFP-Pum1ΔC at 0 and 18 h after resumption of meiosis. Dashed lines outline edge of germinal vesicle (GV). (B) Percentages of oocytes not injected (–) and injected with GFP, GFP–Pum1 (Pum1), GFP–Pum1ΔQN (ΔQN), GFP–Pum1ΔN (ΔN) and GFP–Pum1ΔC (ΔC) that extruded a polar body (means±s.d.; *n*=3). The numbers in parentheses indicate the total numbers of oocytes analyzed. ***P*<0.01 (unpaired *t*-test relative to the oocytes injected with GFP). (C) Immunofluorescence of β-tubulin (red) in oocytes injected with GFP or GFP–Pum1ΔC (Pum1ΔC) at 18 h after resumption of meiosis. DNA is shown in blue. Arrows indicate multiple poles. Similar results were obtained from three independent experiments. (D) FISH analysis of *Mad2* (green) and cyclin B1 (red) mRNAs in oocytes expressing GFP, GFP–Pum1ΔQN (Pum1ΔQN), GFP–Pum1ΔN (Pum1ΔN) and GFP–Pum1ΔC (Pum1ΔC) at 0 and 4 h after resumption of meiosis. (E) The numbers of RNA granules per 100 μm^2 in individual oocytes in D were counted (mean±s.d.). The numbers in parentheses indicate the total numbers of oocytes analyzed. ***P*<0.01, ****P*<0.001 (unpaired *t*-test). (F) Immunoblotting of cyclin B1, Mad2 and γ-tubulin in oocytes not injected (–) and injected with GFP, GFP–Pum1 (Pum1), GFP–Pum1ΔQN (ΔQN), GFP–Pum1ΔN (ΔN) and GFP-Pum1ΔC (ΔC) 4 h after resumption of meiosis. Similar results were obtained from three independent experiments. (G) Immunofluorescence of β-tubulin (red) in oocytes not injected (Control) and injected with GFP, GFP–Pum1ΔC (Pum1ΔC) or GFP–Pum1ΔC followed by the injection with cyclin B1 mRNA (Pum1ΔC+cyclin B1) at 9 h after resumption of meiosis. DNA is shown in blue. GV, germinal vesicle; PB, polar body. Scale bars: 20 μm (A,C,G), 5 μm (D).

Journal of Cell Science (2020) 133, jcs249128. doi:10.1242/jcs.249128

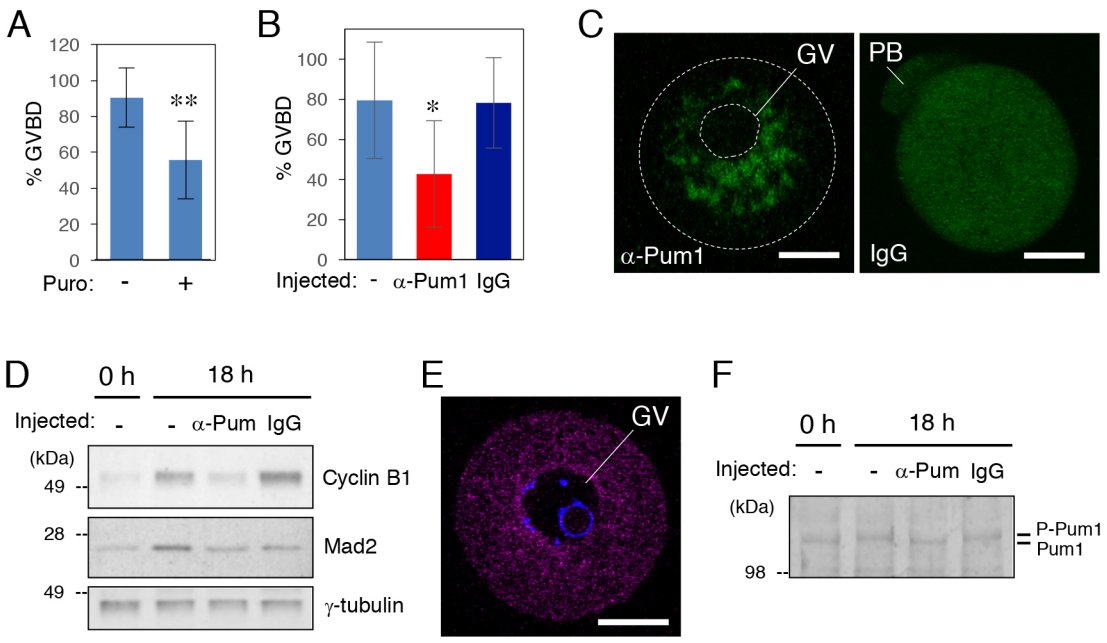

Fig. 7. Stabilization of Pum1 aggregates by anti-Pum1 antibody prevents the translation of target mRNA. (A) Percentages of oocytes incubated with (+) and without (–) puromycin (Puro) that induced GVBD (mean±s.d.; n=3). **P<0.01 (unpaired t-test). (B) Percentages of oocytes not injected (–) and injected with anti-Pum1 antibody (α-Pum1) or control IgG (IgG) that induced GVBD (means±s.d.; n=5). *P<0.05 (unpaired t-test). (C) Distribution of GFP-Pum1 in oocytes injected with anti-Pum1 antibody (α-Pum1) or control IgG (IgG). Dashed lines outline edge of indicated region or oocyte. (D) Immunoblotting of cyclin B1, Mad2 and γ-tubulin in oocytes not injected (–) and injected with anti-Pum1 antibody (α-Pum1) or control IgG (IgG) at 0 and 18 h after resumption of meiosis. Similar results were obtained from two independent experiments. (E) Distribution of the injected anti-Pum1 antibody (magenta). DNA is shown in blue. (F) Immunoblotting of Pum1 in oocytes not injected (–) and injected with anti-Pum1 antibody (α-Pum1) or control IgG (IgG) at 0 and 18 h after resumption of meiosis. Similar results were obtained from two independent experiments. GV, germinal vesicle; PB, polar body. Scale bars: 20 µm.

responsible for Pum1 phosphorylation are present and at least partially active in immature oocytes, and that the dissolution of Pum1 is promoted by phosphorylation. Polo-like kinase (Plk) 1 and 4 have been shown to be present in immature mouse oocytes (Bury et al., 2017; Pahlavan et al., 2000). Interestingly, inhibition of Plk4, but not that of Plk1, prevented the dissolution of Pum1 aggregates (Fig. 8C,D; Fig. S6A). Inhibition of Plk4 also prevented the phosphorylation of Pum1, though Pum1 seemed still partially phosphorylated (Fig. 8B, bottom). Thereby, Plk4 is a kinase promoting the dissolution of Pum1 aggregates and Pum1 phosphorylation in oocytes treated with OA. No effect on the dissolution of Pum1 was observed when activation of mitogen-activated protein kinases (MAPKs) was inhibited with U0126, while aggregate dissolution was delayed but not prevented when the activity of MPF was inhibited with roscovitine (Fig. S6A), suggesting that MPF, which consists of pre-existing cyclin B2 and Cdc2 kinase (Daldello et al., 2019), is partially involved in Pum1 aggregate dissolution. Together, these results provide a link between phosphorylation of Pum1 and dissolution of Pum1 aggregates.

We further analyzed the effects of OA treatment on *Mad2* and cyclin B1 RNA granules and translational activation of these mRNAs. *Mad2* and cyclin B1 RNA granules disappeared almost completely at 2 h after treatment with OA (Fig. 8E,F). In contrast, inhibition of Plk4 prevented the disassembly of both RNA granules (Fig. 8E,F). In addition, OA treatment induced synthesis of Mad2 and cyclin B1, while both proteins were not synthesized in oocytes treated with OA and Plk4 inhibitor (Fig. 8G; Fig. S6B). Taken together, Plk4 rapidly promotes phosphorylation of Pum1, dissolution of Pum1 aggregates, disassembly of *Mad2* and cyclin B1 RNA granules, and translational activation of both mRNAs when PP1 and PP2A activities are inhibited.

To assess the possibility that the anti-Pum1 antibody injected into oocytes prevented phosphorylation of Pum1, we analyzed the Pum1 phosphorylation state in this experiment. Pum1 phosphorylation was observed in oocytes injected with control IgG, while it was prevented in oocytes injected with the anti-Pum1 antibody (Fig. 7F). The results support the importance of Pum1 phosphorylation for dissolution of Pum1 aggregates and translational activation of target mRNAs.

DISCUSSION

Extensive biochemical studies have demonstrated the importance of *cis*-acting mRNA elements and *trans*-acting RNA-binding proteins in the temporal regulation of translation (Radford et al., 2008). However, their cytoplasmic and molecular mechanisms remain largely unknown. Our results provide an aggregation–dissolution model for temporal and spatial control of mRNA translation, that is, Pum1 aggregates in clustered structures ensure translational repression of target mRNAs by stably maintaining their granular structures, and the dissolution of aggregates, possibly mediated by phosphorylation, permits the disassembly of granules and translational activation of mRNAs. Given that many dormant mRNAs stored in oocytes contain PBEs (Chen et al., 2011) and Pum1 targets more than 1000 mRNAs in the testis and brain (Chen et al., 2012), Pum1 would be expected to target a large number of mRNAs in oocytes. In addition, clusters of Pum1 aggregates might comprise granules of these target mRNAs and related proteins, and thereby allow their coordinated regulation. Our results will be a basis for understanding how translational timings of hundreds of mRNAs are coordinately regulated.

Phase changes of Pum1 and translational regulation of target mRNAs

Recent studies have demonstrated that many of the RNA-binding proteins harbor prion-like domains and that some of these proteins

Journal of Cell Science (2020) 133, jcs249128. doi:10.1242/jcs.249128

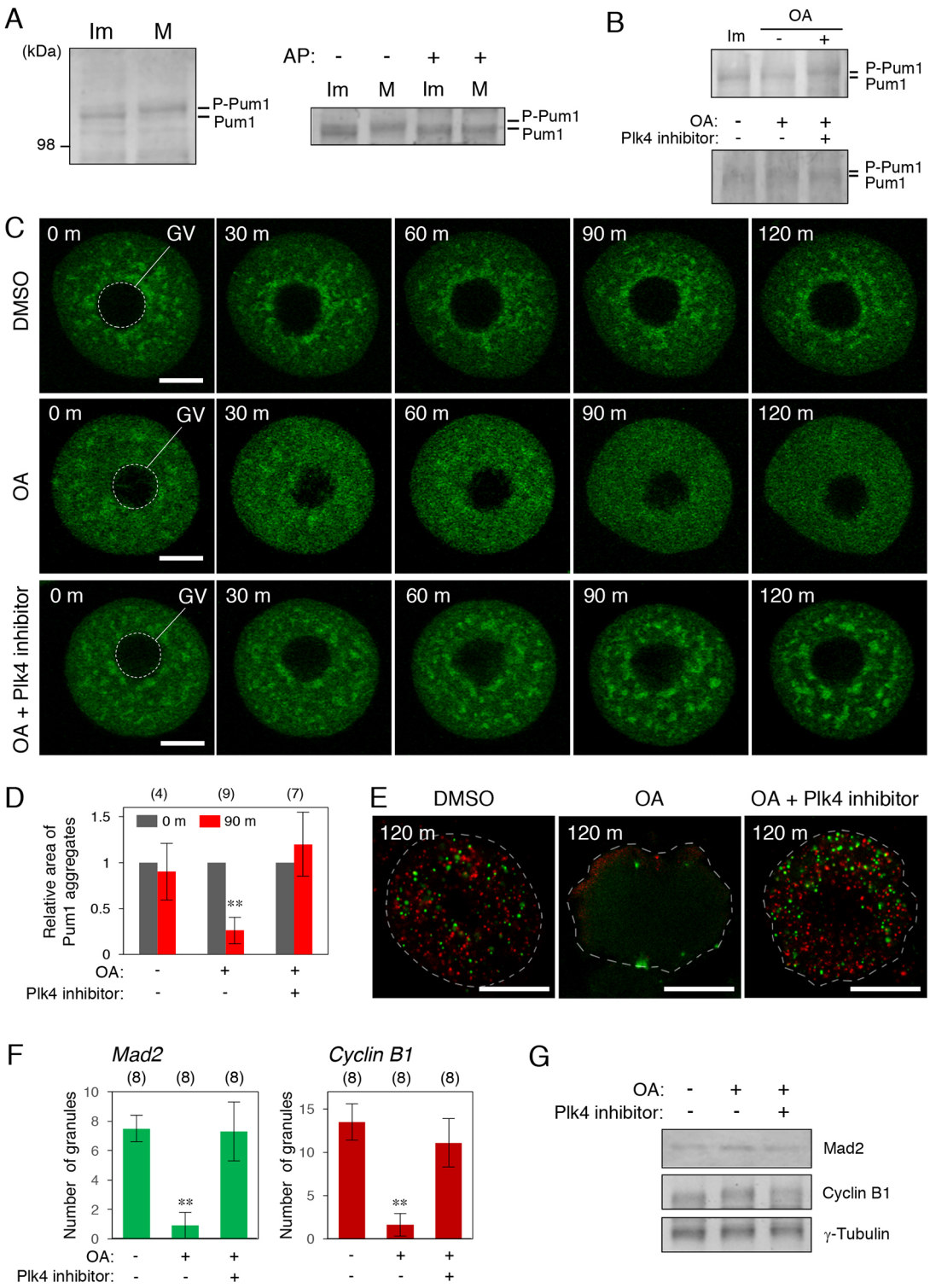

Fig. 8. Phosphorylation of Pum1 is coupled with the dissolution of aggregates, disassembly of RNA granules and translational activation of target mRNAs. (A) Analysis of phosphorylation of Pum1 (P-Pum1). Left, immature (Im) and mature (M) oocytes were analyzed by immunoblotting. Right, immunoblotting after treatment with (+) and without (–) alkaline phosphatase (AP). Similar results were obtained from two independent experiments. (B) Top, Pum1 phosphorylation in oocytes treated with OA (+) or DMSO (–). Similar results were obtained from four independent experiments. Bottom, Pum1 phosphorylation in oocytes at 60 min after treatment with (+) and without (–) OA or Plk4 inhibitor. (C) Time course of GFP–Pum1 in oocytes treated with DMSO, OA, or OA and Plk4 inhibitor for 0–120 min after treatment. Similar results were obtained from three independent experiments. (D) Quantitative analysis (mean±s.d.) of Pum1 aggregates in oocytes treated with (+) and without (–) OA or Plk4 inhibitor. The numbers in parentheses indicate the total numbers of oocytes analyzed. $^{**}P<0.01$ (unpaired *t*-test). (E) FISH analysis of *Mad2* (green) and cyclin B1 (red) mRNAs in oocytes treated with DMSO, OA or OA and Plk4 inhibitor (OA+Plk4 inhibitor) at 120 min after treatment. (F) The numbers of RNA granules per 100 μm^2 in individual oocytes in E were counted (mean±s.d.). The numbers in parentheses indicate the total numbers of oocytes analyzed. $^{**}P<0.01$ (unpaired *t*-test). (G) Immunoblotting of Mad2, cyclin B1 and γ-tubulin in oocytes treated with (+) and without (–) OA or Plk4 inhibitor 120 min after resumption of meiosis. Similar results were obtained from three independent experiments. Dashed lines outline edge of indicated region or oocyte. GV, germinal vesicle. Scale bars: 20 μm.

Journal of Cell Science (2020) 133, jcs249128. doi:10.1242/jcs.249128

have the ability to assemble RNA granules (Decker et al., 2007; Gilks et al., 2004; Reijns et al., 2008). These RNA-binding proteins were shown to promote liquid–liquid phase separation, resulting in the assembly of protein–RNA complexes into droplets (Elbaum-Garfinkle et al., 2015; Lin et al., 2015; Molliex et al., 2015; Nott et al., 2015). These droplets are thought to function as partitions that effectively maintain stability and/or translational repression of mRNAs. In contrast, phase transition of the liquid droplets into solid-like structures such as amyloid fibrils has been thought to contribute to pathological diseases such as amyotrophic lateral sclerosis (ALS) (Li et al., 2013; Weber and Brangwynne, 2012). However, more recently, solid granules were found to assemble during muscle regeneration in a physical state (Vogler et al., 2018). In addition, core regions of stress granules were shown to exhibit solid-like properties (Jain et al., 2016; Shiina, 2019). Although these findings suggest the involvement of solid granules in RNA regulation, the physiological importance of the phase changes of protein aggregation from liquid to solid states and vice versa remains unclear.

In this study, we demonstrated that Pum1 assembled into aggregates in highly clustered structures through the Q/N-rich region and that these aggregates showed insoluble and immobile properties in immature oocytes (Figs 3 and 4). After initiation of oocyte maturation, the Pum1 aggregates dissolved into a soluble and mobile state (Figs. 4A and 5). The mutant form of Pum1 that lacks the C-terminal PUF domain, Pum1ΔC, formed stable aggregates and these structures persisted after initiation of oocyte maturation (Fig. 6A; Fig. S2G). Pum1ΔC is expected to be unable to bind to target mRNAs but to have the ability to form assemblies via the Q/N-rich region. Since it has been shown that RNA molecules can ‘buffer’ the assembly of RNA-binding proteins that harbor prion-like domains into solid-like aggregates (Maharana et al., 2018), it is possible that the lack of the RNA-binding ability of Pum1ΔC results in the assembly of large and stable aggregates, as in the case of RNA-binding proteins such as TDP43 and FUS. Pum1ΔC would stabilize endogenous Pum1 aggregates via Q/N-rich region-mediated assembly into or around endogenous Pum1 aggregates, and thereby prevent the translational activation of Pum1-target mRNAs (Fig. 6). The anti-Pum1 antibody also prevented dissociation of Pum1 aggregates and synthesis of cyclin B1 and Mad2 (Fig. 7). This antibody could act to stabilize Pum1 aggregates by inhibiting Pum1 phosphorylation (Fig. 7F) as discussed below, although we cannot rule out a possibility that the antibody affected the conformation or composition of Pum1 assemblies. Collectively, our results suggest a physiological significance of phase changes of protein aggregation in translational repression and activation of target mRNAs.

Regulation of the subcellular structures and states of Pum1 by phosphorylation and dephosphorylation

P granules are the germinal granules in *C. elegans* that are important for fate decisions of germline cells. Live imaging of embryos demonstrated that P granules behave as dynamic liquid droplets (Brangwynne et al., 2009). Intriguingly, disassembly of *C. elegans* P granules after fertilization has been shown to require MBK-2 kinase, while subsequent assembly of P granules at the posterior region of embryos requires protein phosphatase 2A (PP2A) (Gallo et al., 2010; Wang et al., 2014). MEG-1 and MEG-3 were found to be the substrates of MBK-2 and PP2A in the granules (Wang et al., 2014). These results demonstrated that the dynamics of liquid RNA granules is regulated by phosphorylation and dephosphorylation of assembled proteins.

Our results suggest the importance of protein phosphorylation and dephosphorylation for changes in structures and states of Pum1 aggregates. SDS-PAGE analysis demonstrated that Pum1 was phosphorylated during mouse oocyte maturation (Fig. 8A). Interestingly, treatment of oocytes with OA, an inhibitor of PP1 and PP2A, led to rapid dissociation of Pum1 aggregates and induced Pum1 phosphorylation (Fig. 8B–D). Since PP2A was shown to be localized in the cytoplasm of GV-stage mouse oocytes, while PP1 was dominantly localized in the nucleus (Smith et al., 1998), PP2A would be a phosphatase involved in Pum1 dephosphorylation and the maintenance of Pum1 aggregates. Even when the activity of PP1 and PP2A was inhibited by OA, Pum1 phosphorylation was attenuated and the aggregates persisted in the presence of a Plk4 inhibitor (Fig. 8B–D), suggesting that Plk4 is a kinase responsible for Pum1 phosphorylation and aggregate dissolution. However, it is likely that other kinases phosphorylate Pum1, since inhibition of Plk4 activity delayed, but did not completely prevent, the dissolution of Pum1 aggregates and Pum1 phosphorylation after initiation of oocyte maturation (unpublished data). To date, only Nemo-like kinase 1 (Nlk1) has been shown to phosphorylate Pum1 (Ota et al., 2011b). Our results suggest the participation of MPF in the dissolution of Pum1 aggregates (Fig. S6A). Involvement of Nlk1, MPF and other kinases in phosphorylation of Pum1 and dissolution of aggregates remains to be investigated. Puf3, one of the PUF family proteins in yeast, was shown to be phosphorylated at more than 20 sites throughout the entire region (Lee and Tu, 2015). In addition, we previously showed that Pum1 was phosphorylated at multiple sites in an early period of oocyte maturation in zebrafish (Saitoh et al., 2018). These results suggest that many sites, including those in the Q/N-rich domain, might be phosphorylated, resulting in Pum1 aggregate dissolution.

The anti-Pum1 antibody injected into GV-stage oocytes prevented the Pum1 phosphorylation, aggregate dissolution, and synthesis of cyclin B1 and Mad2 (Fig. 7). Since this antibody recognizes amino acid residues from 225 to 275 of Pum1, phosphorylation around this region might be crucial for triggering dissolution of Pum1 aggregates. We previously showed that overexpression of GFP–Pum1ΔC prevented disassembly of RNA granules and phosphorylation of endogenous Pum1 in zebrafish oocytes (Saitoh et al., 2018). Correctively, these results support the notion that phosphorylation of Pum1 is a critical step in promoting dissolution of Pum1 aggregates, disassembly of RNA granules, and translational activation of Pum1-target mRNAs.

Subcellular structures of Pum1 and homogenous RNA granules

An intriguing finding in this study is that the Pum1-target *Mad2* and cyclin B1 mRNAs formed distinct granules in the oocyte cytoplasm, instead of making granules containing both mRNAs (Fig. 2). Pum1 was found to produce highly clustered structures that surrounded both *Mad2* and cyclin B1 RNA granules (Fig. 3). These structures partially resemble those of germ granules in *Drosophila* embryos, in which mRNAs form homogenous RNA clusters and are spatially positioned within the granules, while RNA-binding proteins are evenly distributed throughout the granules (Trcek et al., 2015). These findings suggest the existence of a common mechanism by which each mRNA could be organized into homogenous particles. However, in contrast to our findings, the structures of *Drosophila* germ granules were not changed during early stages of embryogenesis and were independent of the control of mRNA translation and degradation (Trcek et al., 2015). Therefore, the function of spatially organized structures of germ granules in

Journal of Cell Science (2020) 133, jcs249128. doi:10.1242/jcs.249128

Drosophila embryos seems to be different from the function of subcellular structures of Pum1 and RNA granules in mouse oocytes.

Our results showed that Pum1 aggregates surrounded and overlapped *Mad2* and cyclin B1 RNA granules at the periphery but were rarely localized at the center of granules (Fig. 3). Given that Pum1 was shown to bind directly to PBE in the 3′UTR of target mRNAs including cyclin B1 (Kotani et al., 2013; Nakahata et al., 2003; Ota et al., 2011a; Piqué et al., 2008), Pum1-target mRNAs may form highly ordered structures within granules in which the 3′ ends of mRNAs are localized at the periphery of granules, as in the case of the long noncoding RNA, *Neat1*, in paraspeckle nuclear bodies (Souquere et al., 2010; West et al., 2016). In a small proportion of cyclin B1 and *Mad2* RNA granules, Pum1 was localized at the center of granules. Since this type of localization was found in large granules, the central localization may result from co-localization of several granules that are surrounded by Pum1. Structural analysis of the RNA granules will be an interesting issue to be explored.

Details of the molecular mechanisms by which Pum1 is assembled into aggregates remain unknown. One possible model is that Pum1 binds to a target mRNA via the PUF domain and subsequently assembles into aggregates via the Q/N-rich region. Another possibility is that Pum1 contains two populations; one population binds to target mRNAs and the other functions as structural scaffolds without binding to mRNAs. In addition to the homogenous assembly of Pum1, heterogenous assembly with other RNA-binding proteins may produce aggregates. In any case, the resulting Pum1 aggregates in clustered structures would make compartments that function as regulatory units with related proteins assembled together. These units would enable the coordinate regulation of the translation of assembled mRNAs. In various cells besides oocytes, many mRNAs are known to be transported and localized at subcellular regions through binding of RNA-binding proteins to mainly 3′UTRs (Martin and Ephrussi, 2009; Mili and Macara, 2009; Russo et al., 2008). Recent studies have demonstrated the translationally repressed mRNAs accumulate at protrusions of fibroblast cells and synapses of neuronal cells in a static state (Buxbaum et al., 2014; Moissoglu et al., 2019). Since Pum1 functions in diverse systems and other RNA-binding proteins that harbor prion-like domains may function in a manner similar to that of Pum1, our results will contribute to an understanding of the nature of temporal and spatial control of translation in many cell types of diverse organisms.

MATERIALS AND METHODS

Preparation of ovaries and oocytes

All animal experiments in this study were approved by the Committee on Animal Experimentation, Hokkaido University. Mouse ovaries were dissected from 8-week-old females in M2 medium (Sigma). Oocytes were retrieved from ovaries by puncturing the ovaries with a needle in M2 medium containing 10 µM milrinone (Fujifilm Wako Pure Chemical), which prevents resumption of oocyte maturation. To induce oocyte maturation, the isolated oocytes were washed three times and incubated with M2 medium without milrinone at 37°C. Alternatively, oocyte maturation was induced by injection of 5 U of human chorionic gonadotropin (hCG; Kyoritsu Seiyaku) 48 h after injection of 5 U of pregnant mare serum gonadotropin into 3-week-old females. For RT-PCR and poly(A) test (PAT) assays, ovaries and oocytes were extracted with Trizol reagent (Invitrogen) and total RNA was used for RT-PCR and RNA ligation-coupled RT-PCR. For *in situ* hybridization analysis, mouse ovaries were fixed with 4% paraformaldehyde in PBS (137 mM NaCl, 2.7 mM KCL, 10 mM Na_2HPO_4, and 2 mM KH_2PO_4, pH 7.2) (4% PFA/PBS) overnight at 4°C. Oocytes isolated from ovaries were transferred into oviducts after fixation with 4% PFA/PBS for 10 min at 4°C. The oviducts were then fixed with 4% PFA/PBS overnight at 4°C. For immunoblotting analysis, 30 oocytes were washed with PBS and extracted with lithium dodecylsulfate (LDS) sample buffer (Novex) at 0, 10 and 18 h after resumption of oocyte maturation. For immunoprecipitation and RT-PCR analysis, mouse ovaries were homogenized with an equal volume of ice-cold extraction buffer (EB; 100 mM β-glycerophosphate, 20 mM HEPES pH 7.5, 15 mM $MgCl_2$, 5 mM EGTA, 1 mM dithiothreitol, 100 µM PMSF and 3 µg/ml leupeptin) containing 1% Tween 20 and 100 U/ml RNasin Plus RNase inhibitor (Promega). After centrifugation at 15,000 ***g*** for 10 min at 4°C, the supernatant was collected and used for immunoprecipitation.

Zebrafish ovaries were dissected from adult females in zebrafish Ringer's solution (116 mM NaCl, 2.9 mM KCl, 1.8 mM $CaCl_2$, and 5 mM HEPES; pH 7.2). Zebrafish oocytes were manually isolated from ovaries with forceps under a dissecting microscope. Oocyte maturation was induced by treatment with 1 µg/ml of 17α,20β-dihydroxy-4-pregnen-3-one (Toronto Research Chemicals), a maturation-inducing hormone (MIH) in fish. For ultracentrifugation analysis, fully grown immature oocytes and oocytes 3 h after MIH stimulation (matured oocytes) were homogenized with an equal volume of ice-cold EB containing 0.2% Tween 20. After ultracentrifugation using an S100AT6 rotor at 90,000 ***g*** for 30 min at 4°C, the supernatant and precipitates were collected and used for immunoblot analysis.

RT-PCR and quantitative PCR

Total RNA extracted from mouse ovaries or 50 immature oocytes was used for cDNA synthesis using the Super Script III First Strand Synthesis System (Invitrogen). The full length of *Mad2* mRNA was amplified with the cDNA and primer sets specific to *Mad2*, m*Mad2*-f1 (5′-GTAGTGTTCTCCGTT-CGATCTAG-3′) and m*Mad2*-r1 (5′-GTATCACTGACTTTTAAAGCTTG-ATTTTTA-3′). The amounts of short and long *Mad2* mRNAs were quantified by using a real-time PCR system with SYBR green PCR Master Mix (Applied Biosystems) according to the manufacturer's instructions. The short and long *Mad2* transcripts were amplified with the cDNA and primer sets to both types of *Mad2*, m*Mad2*-f2 (5′-GAATAGTATGGTGGCCTACAA-3′) and m*Mad2*-r2 (5′-TTCCCTCGTTTCAGGCACCA-3′), and primer sets specific to long *Mad2*, m*Mad2*-f3 (5′-CTGGACCAGGATATAAAGAAGCG-3′) and m*Mad2*-r3 (5′-GCTGTCCTCCCTGCCTCTCT-3′). The signals obtained with distinct primer sets were normalized with standard curves obtained with plasmid DNAs encoding the short or long *Mad2* gene.

Section *in situ* hybridization

Section *in situ* hybridization and fluorescent *in situ* hybridization (FISH) with the tyramide signal amplification (TSA) Plus DNP system (PerkinElmer) were performed according to the procedure reported previously (Takei et al., 2018). Briefly, fixed ovaries or oviducts containing oocytes isolated from ovaries were dehydrated, embedded in paraffin and cut into 7-µm-thick sections. Digoxigenin (DIG)-labeled antisense RNA probes for the full length of short *Mad2* and sequences specific to long *Mad2* were used for detection of *Mad2* gene transcripts. No signal was detected with sense probes. After hybridization and washing, samples were incubated with an anti-DIG-horseradish peroxidase (HRP) antibody (Roche, cat. no. 11 633 716 001; 1:500 dilution) for 30 min. To detect *Mad2* transcripts by alkaline phosphatase (AP) staining, a reaction with tyramide–dinitrophenyl (DNP) (PerkinElmer) was performed according to the manufacturer's instructions. The samples were then incubated with an anti-DNP-AP antibody (PerkinElmer cat. no. NEL746A; 1:500 dilution) for 30 min, followed by reaction with NBT and BCIP according to the manufacturer's instructions. To detect *Mad2* transcripts by fluorescence microscopy, a reaction with tyramide–fluorescein (PerkinElmer) was performed according to the manufacturer's instructions. To detect nuclei, samples were incubated with 10 µg/ml Hoechst 33258 for 10 min. After being mounted with a Prolong Antifade Kit (Molecular Probes), the samples were observed under an LSM5 LIVE confocal microscope (Carl Zeiss) at room temperature using a Plan Apochromat 63×/1.4 NA oil differential interference contrast lens and LSM 5 DUO 4.2 software (Carl Zeiss).

Double *in situ* hybridization of *Mad2* and cyclin B1 transcripts was performed as follows. A fluorescein-labeled antisense RNA probe for cyclin B1 was used for detection of the cyclin B1 gene transcript. Sections (7-µm-

thick) of mouse ovaries were hybridized with a mixture of *Mad2* and cyclin B1 antisense RNA probes. Then the samples were incubated with an anti-fluorescein–HRP antibody (Roche, cat. no. 11 426 346 910; 1:200 dilution) for 30 min. Reaction with tyramide–Cy3 (PerkinElmer) was performed according to the manufacturer's instructions. For inactivating HRP, samples were incubated with 1% H_2O_2 in PBS for 15 min. Detection of the DIG-labeled antisense *Mad2* RNA probe was performed as described above. After staining with Hoechst 33258, the samples were mounted and observed under the LSM5 LIVE confocal microscope. The number of *Mad2* and cyclin B1 RNA granules was quantified using ImageJ software, which enables detection of granules according to size (larger than 0.2 µm) and intensity at the center of granules. Similar results were obtained using a fluorescein-labeled antisense RNA probe for *Mad2* and a DIG-labeled RNA probe for cyclin B1.

Immunoblotting

Mouse oocyte extracts were separated by SDS-PAGE with Bolt Bis-Tris Plus Gels (Novex), blotted onto an Immobilon membrane using a Bolt Mini Blot Module (Novex), and probed with an anti-human Pum1 goat antibody (Bethyl Laboratories, cat. no. A300-201A; 1:1000 dilution), an anti-human cyclin B1 rabbit antibody (Santa Cruz Biotechnology, Inc., cat. no. sc-752; 1:100 dilution), an anti-hamster cyclin B1 mouse monoclonal antibody (V152, Abcam, cat. no. ab72; 1:1000 dilution), and an anti-human Mad2 rabbit antibody (Bethyl Laboratories, Inc., cat. no. A300-301A; 1:1000 dilution). The supernatant and precipitates of zebrafish oocyte extracts were separated by SDS-PAGE, blotted onto an Immobilon membrane, and probed with an anti-*Xenopus* Pum1 mouse monoclonal antibody (Pum2A5, Nakahata et al., 2001; 1:1000 dilution) and an anti-GM130 mouse monoclonal antibody (BD Biosciences, cat. no. 610822; 1:250). The intensity of signals was quantified using ImageJ software.

Poly(A) test assay

RNA ligation-coupled RT-PCR was performed according to the procedure reported previously (Kotani et al., 2013). Four hundred ng of total RNA extracted from pools of 250 mouse oocytes was ligated to 400 ng of P1 anchor primer [5′-P (phosphate)-GGTCACCTTGATCTGAAGC-NH_2-3′] in a 10-µl reaction using T4 RNA ligase (New England Biolabs) for 30 min at 37°C. The ligase was inactivated for 5 min at 92°C. Eight µl of the RNA ligation reaction was used in a 20-µl reverse transcription reaction using the Superscript III First Strand Synthesis System with a P1′ primer (5′-GCTTCAGATCAAGGT-GACCTTTTTTTT-3′). A total of 2 µl of the cDNA was used for the first PCR with the P1′ primer and an m*Mad2*-f4 primer (5′-GACCCCATATT-GAAATACATGC-3′) or mcyclin B1-f1 primer (5′-CCACTCCTGTCTTG-TAATGC-3′) for 45 cycles. Then, 1 µl of the first PCR was used for the second PCR with the IRD800-P1′ primer (5′-IRD800-GCTTCAGATCAAGGTGA-CCTTTTTTTT-3′) and an m*Mad2*-f5 primer (5′-GAGCTCACAACGCA-GTTG-3′) or mcyclin B1-f2 primer (5′-CCTGGAAAAGAATCCTGTCTC-3′) for 20 cycles. The PCR product was resolved on a 3% TAE gel and observed by using Odyssey (M&S TechnoSystem). We confirmed that the increase in PCR product length was due to elongation of the poly(A) tails by cloning the second PCR products and sequencing them.

RT-PCR analysis after immunoprecipitation

A total of 80 µl of mouse ovary extracts was incubated with 4 µl of 1.0 µg/ml anti-human Pum1 goat antibody (Bethyl Laboratories, cat. no. A300-201A) or 4 µl of 1.0 µg/ml control goat IgG (Jackson, cat. no. 005-000-003) for 1 h at 4°C. The extracts were then incubated with protein A–Sepharose beads (GE Healthcare) for 3 h at 4°C and washed five times with EB containing 1% Tween 20. After extraction of mRNAs from the beads with Trizol reagent, RT-PCR was performed using primer sets specific to *Mad2*, m*Mad2*-f6 (5′-GTGACCATTGTTAAAGGAATCCATCCC-3′) and m*Mad2*-r1, to cyclin B1, mcyclin B1-f3 (5′-AGTCCCTCACCCTCCCAAAAGC-3′) and mcyclin B1-r1 (5′-AAAGCTTTCCACCAATAAATTTTATTCAAC-3′), to β-actin, mβ-actin-f1 (5′-AGTCCCTCACCCTCCCAAAAGC-3′) and mβ-actin-r1 (5′-GGTCTCAAGTCAGTGTACAGGC-3′), and to α-tubulin, mα-tubulin-f1 (5′-CTTTGTGCACTGGTATGTGGGT-3′) and mα-tubulin-r1 (5′-ATA-AGTGAAATGGGCAGCTTGGGT-3′). The intensity of signals was quantified using ImageJ software.

Immunofluorescence

Fixed ovaries were dehydrated, embedded in paraffin, and cut into 7-µm-thick sections. After rehydration, samples were microwaved for 10 min (500 W) with 0.01 M citric acid (pH 6.0) containing 0.05% Tween 20, followed by cooling down for 40 min. After incubation with a TNB blocking solution (PerkinElmer) for 1 h at room temperature, the samples were incubated with anti-human Pum1 goat antibody (Novus Biologicals, cat. no. NB100-259; 1:100 dilution) at 4°C for overnight. The samples were then incubated with anti-goat IgG-Alexa Fluor Plus 647 antibody (Invitrogen, cat. no. A32849; 1:200 dilution) at room temperature for 1 h. After staining with Hoechst 33258, the samples were mounted and observed under the LSM 5 LIVE confocal microscope. No signal was detected in the reaction without the anti-Pum1 antibody. To further confirm the specificity of signals, a GST-fused N-terminus fragment of mouse Pum1 (amino acids 1–399) (GST-Pum1NN) was expressed in *Escherichia coli* and gel-purified. Before immunostaining of mouse ovary sections, 3 µg of anti-Pum1 antibody was incubated with 18 µg of GST-Pum1NN in PBS (300 µl reaction) for overnight at 4°C. To simultaneously detect Pum1 and cyclin B1 and *Mad2* mRNAs, the samples were immunostained with the Pum1 antibody as described above after detection of the cyclin B1 and *Mad2* RNA probes in *in situ* hybridization analysis. The intensities of signals were measured by ImageJ software. Monte Carlo simulation was performed with ImageJ software by creating random dots and measuring distance to Pum1 aggregates. The dimension of the images used was 5000×5000 nm.

mRNA injection and immunostaining

Sequences encoding the full-length and portions of mouse Pum1 (ΔQN, ΔN and ΔC) were cloned into pCS2-GFP-N to produce Pum1 fused with GFP at the N-terminus of Pum1. mRNAs encoding GFP, GFP–Pum1, GFP–Pum1ΔQN, GFP–Pum1ΔN, and GFP–Pum1ΔC were synthesized with an mMESSAGE mMACHINE SP6 kit (Life Technologies) and dissolved in distilled water. Then, 10 pg of the mRNAs was injected into fully grown mouse oocytes using an IM-9B microinjector (Narishige) under a Dmi8 microscope (Leica) in M2 medium containing 10 µM milrinone. After being incubated for 4 h at 37°C, the oocytes were fixed with 2% PFA/PBS containing 0.05% Triton X-100 for 1 h at 4°C for *in situ* hybridization analysis or were washed four times with M2 medium without milrinone for induction of oocyte maturation. At the appropriate time points after resumption of meiosis, the distribution of proteins fused with GFP was observed under the LSM 5 LIVE confocal microscope. To simultaneously detect GFP–Pum1 and cyclin B1 or *Mad2* mRNA, the fixed oocytes were attached on slide glasses using Smear Gell (GenoStaff). The oocytes were immunostained with anti-GFP mouse antibody (Roche, cat. no 1 814 460; 1:200 dilution) followed by anti-mouse IgG-Alexa Fluor 488 antibody (Molecular Probes; 1:200 dilution) after hybridization and washing of the cyclin B1 or *Mad2* RNA probe in *in situ* hybridization analysis.

To analyze the effects of permeabilization on GFP–Pum1 aggregates, the oocytes injected with mRNA encoding GFP or GFP–Pum1 were incubated for overnight at 37°C with M2 medium containing 10 µM milrinone. After observation under the LSM 5 LIVE confocal microscope, the oocytes were transferred to M2 medium containing 0.012% digitonin and 10 µM milrinone. The oocytes were then observed under the confocal microscope at the appropriate time points.

To analyze the effects of GFP–Pum1ΔC on oocyte maturation, the oocytes injected with mRNA encoding GFP or GFP–Pum1ΔC were incubated for 9 and 18 h at 37°C with M2 medium and then fixed with 4% PFA/PBS for 1 h at 37°C. The samples were permeabilized with PBS containing 0.1% Triton X-100 for 20 min, followed by incubation with a blocking/washing solution (PBS containing 0.3% BSA and 0.01% Tween 20) for 1 h at room temperature. The samples were then incubated with Cy3-conjugated anti-β-tubulin antibody (Sigma, cat. no. C4585; 1:150 dilution) for 30 min at room temperature, washed with washing solution, and mounted with VECTASHIELD mounting medium with DAPI (Funakoshi). The samples were observed under the LSM 5 LIVE confocal microscope.

To analyze the stability of Mad2 in immature and mature oocytes, 2.5 pg of mRNA encoding GFP–Mad2 was injected into GV- and MII-stage oocytes. After being incubated for 2 h at 37°C, the oocytes were treated with puromycin and observed under the Nikon Ti-E inverted microscope equipped with the Nikon A1Rsi special imaging confocal laser scanning system.

FRAP analysis

FRAP measurements were performed according to the procedure reported previously (Kimura and Cook, 2001; Tsutsumi et al., 2016). A Nikon Ti-E inverted microscope equipped with a Nikon A1Rsi special imaging confocal laser scanning system (Nikon) was used for the measurements. A small area (~10 µm diameter circle) was positioned in a region of the oocyte cytoplasm and bleached using 100% 488 nm laser with five scans. Images were then collected using 1.0% laser power every 5.0 s for 5.0 min. The relative fluorescence intensity in the bleached area was normalized using the intensity in the control area measured subsequently after measurement of the bleached area. The normalized intensities were analyzed using a fitting equation for a double exponential association model. A smaller bleached area (5 µm diameter circle) gave equivalent results. To observe details of changes in GFP–Pum1 aggregates after photobleaching, similar experiments were performed using a high-resolution microscope, Zeiss LSM 980 with Airyscan 2 Multiplex (Carl Zeiss).

Puromycin treatment and Pum1 antibody injection

To inhibit protein synthesis, oocytes were treated with 20 µM puromycin in M2 medium and incubated at 37°C. The oocytes were collected at appropriate time points after incubation with puromycin for immunoblotting analysis. A total of 2 pg of anti-Pum1 antibody (Bethyl Laboratories, cat. no. A300-201A) was injected into fully grown mouse oocytes using the microinjector in M2 medium containing 10 µM milrinone. The oocytes were then washed three times and incubated for 18 h at 37°C with M2 medium containing 1 µM milrinone. To analyze the distribution of GFP–Pum1, 10 pg of the GFP–Pum1 mRNA was co-injected with 2 pg of anti-Pum1 antibody into fully grown mouse oocytes, followed by washing and incubation of oocytes as described above. The distribution of GFP–Pum1 was observed under the LSM 5 LIVE confocal microscope.

Phosphatase treatment

The dephosphorylation experiments were performed according to the procedure reported previously (Pahlavan et al., 2000). Briefly, samples of 30 oocytes in phosphatase buffer (New England Biolabs) containing 1% SDS, 100 µM PMSF and 3 µg/ml leupeptin were incubated with 17.5 U alkaline phosphatase (New England Biolabs) at 37°C for 1 h. The reaction was stopped by adding an equal volume of LDS sample buffer. The samples were then analyzed by immunoblotting.

Okadaic acid, BI2536, centrinone, U0126 and roscovitine treatment

To inhibit activities of protein phosphatase 1 and 2A, oocytes were treated with 2.5 µM okadaic acid (OA; Fujifilm Wako Pure Chemical) in M2 medium containing 10 µM milrinone and incubated at 37°C. OA was dissolved in DMSO as stocks and diluted in M2 medium before use. As a control, oocytes were treated with DMSO. The oocytes were collected at 16 h after incubation for immunoblotting analysis. To analyze the distribution of GFP–Pum1, fully grown mouse oocytes were injected with 10 pg of the GFP–Pum1 mRNA and incubated in M2 medium containing 10 µM milrinone at 37°C for 4 h, followed by treatment with OA as described above. The distribution of GFP–Pum1 was observed under the LSM 5 LIVE confocal microscope. Activities of Plk1 and Plk4 were inhibited by treating the oocytes with 100 nM BI2536 (Chemscene) and 5 µM centrinone (Medchemexpress), respectively, according to the procedure reported previously (Bury et al., 2017). Activities of MAPKs and MPF were inhibited by treating the oocytes with 50 µM U0126 (Abcam) and 50 µM roscovitine (Fujifilm Wako Pure Chemical), respectively, according to the procedure reported previously (Nabti et al., 2014).

Acknowledgements

We thank Drs K. Kobayashi and M. Tsutsumi for technical advice on FRAP analysis. We also thank Dr H. Maita for advice on the detection of PCR amplification in the PAT assay.

Competing interests

The authors declare no competing or financial interests.

Author contributions

Conceptualization: N.T., Y.T., S.K., T.K.; Investigation: N.T., Y.T., S.K., K.S., A.S.; Resources: J.B., W.S.Y., J.C.; Writing - original draft: T.K.; Writing - review & editing: J.C., T.K.; Supervision: T.K.; Project administration: T.K.; Funding acquisition: T.K.

Funding

This work was supported by Grant-in-Aid for Scientific Research (16K07242 to T.K.) from the Ministry of Education, Culture, Sports, Science and Technology, Japan and was in part supported by grants from Takeda Science Foundation, Daiichi Sankyo Foundation of Life Science, Suhara Memorial Foundation, and Japan Society for the Promotion of Science (JSPS) KAKENHI grant number JP16H06280.

Supplementary information

Supplementary information available online at
https://jcs.biologists.org/lookup/doi/10.1242/jcs.249128.supplemental

Peer review history

The peer review history is available online at
https://jcs.biologists.org/lookup/doi/10.1242/jcs.249128.reviewer-comments.pdf

References

Asaoka-Taguchi, M., Yamada, M., Nakamura, A., Hanyu, K. and Kobayashi, S. (1999). Maternal Pumilio acts together with Nanos in germline development in Drosophila embryos. *Nat. Cell Biol.* **1**, 431-437. doi:10.1038/15666

Barkoff, A. F., Dickson, K. S., Gray, N. K. and Wickens, M. (2000). Translational control of cyclin B1 mRNA during meiotic maturation: coordinated repression and cytoplasmic polyadenylation. *Dev. Biol.* **220**, 97-109. doi:10.1006/dbio.2000.9613

Bialojan, C. and Takai, A. (1988). Inhibitory effect of a marine-sponge toxin, okadaic acid, on protein phosphatases. *Biochem. J.* **256**, 283-290. doi:10.1042/bj2560283

Brangwynne, C. P., Eckmann, C. R., Courson, D. S., Rybarska, A., Hoege, C., Gharakhani, J., Julicher, F. and Hyman, A. A. (2009). Germline P granules are liquid droplets that localize by controlled dissolution/condensation. *Science* **324**, 1729-1732. doi:10.1126/science.1172046

Bury, L., Coelho, P. A., Simeone, A., Ferries, S., Eyers, C. E., Eyers, P. A., Zernicka-Goetz, M. and Glover, D. M. (2017). Plk4 and Aurora A cooperate in the initiation of acentriolar spindle assembly in mammalian oocytes. *J. Cell Biol.* **216**, 3571-3590. doi:10.1083/jcb.201606077

Buxbaum, A. R., Wu, B. and Singer, R. H. (2014). Single β-actin mRNA detection in neurons reveals a mechanism for regulating its translatability. *Science* **343**, 419-422. doi:10.1126/science.1242939

Buxbaum, A. R., Haimovich, G. and Singer, R. H. (2015). In the right place at the right time: visualizing and understanding mRNA localization. *Nat. Rev. Mol. Cell Biol.* **16**, 95-109. doi:10.1038/nrm3918

Chen, J., Melton, C., Suh, N., Oh, J. S., Horner, K., Xie, F., Sette, C., Blelloch, R. and Conti, M. (2011). Genome-wide analysis of translation reveals a critical role for deleted in azoospermia-like (Dazl) at the oocyte-to-zygote transition. *Genes Dev.* **25**, 755-766. doi:10.1101/gad.2028911

Chen, D., Zheng, W., Lin, A., Uyhazi, K., Zhao, H. and Lin, H. (2012). Pumilio 1 suppresses multiple activators of p53 to safeguard spermatogenesis. *Curr. Biol.* **22**, 420-425. doi:10.1016/j.cub.2012.01.039

Daldello, E. M., Luong, X. G., Yang, C. R., Kuhn, J. and Conti, M. (2019). Cyclin B2 is required for progression through meiosis in mouse oocytes. *Development* **146**, dev172734. doi:10.1242/dev.172734

Davydenko, O., Schultz, R. M. and Lampson, M. A. (2013). Increased CDK1 activity determines the timing of kinetochore-microtubule attachments in meiosis I. *J. Cell Biol.* **202**, 221-229. doi:10.1083/jcb.201303019

de Moor, C. H. and Richter, J. D. (1999). Cytoplasmic polyadenylation elements mediate masking and unmasking of cyclin B1 mRNA. *EMBO J.* **18**, 2294-2303. doi:10.1093/emboj/18.8.2294

Decker, C. J., Teixeira, D. and Parker, R. (2007). Edc3p and a glutamine/asparagine-rich domain of Lsm4p function in processing body assembly in Saccharomyces cerevisiae. *J. Cell Biol.* **179**, 437-449. doi:10.1083/jcb.200704147

Elbaum-Garfinkle, S., Kim, Y., Szczepaniak, K., Chen, C. C., Eckmann, C. R., Myong, S. and Brangwynne, C. P. (2015). The disordered P granule protein LAF-1 drives phase separation into droplets with tunable viscosity and dynamics. *Proc. Natl. Acad. Sci. USA* **112**, 7189-7194. doi:10.1073/pnas.1504822112

Gallo, C. M., Wang, J. T., Motegi, F. and Seydoux, G. (2010). Cytoplasmic partitioning of P granule components is not required to specify the germline in C. elegans. *Science* **330**, 1685-1689. doi:10.1126/science.1193697

Gebauer, F., Xu, W., Cooper, G. M. and Richter, J. D. (1994). Translational control by cytoplasmic polyadenylation of c-mos mRNA is necessary for oocyte maturation in the mouse. *EMBO J.* **13**, 5712-5720. doi:10.1002/j.1460-2075.1994.tb06909.x

Gennarino, V. A., Singh, R. K., White, J. J., De Maio, A., Han, K., Kim, J. Y., Jafar-Nejad, P., di Ronza, A., Kang, H., Sayegh, L. S. et al. (2015). Pumilio1

haploinsufficiency leads to SCA1-like neurodegeneration by increasing wild-type Ataxin1 levels. *Cell* **160**, 1087-1098. doi:10.1016/j.cell.2015.02.012
Gilks, N., Kedersha, N., Ayodele, M., Shen, L., Stoecklin, G., Dember, L. M. and Anderson, P. (2004). Stress granule assembly is mediated by prion-like aggregation of TIA-1. *Mol. Biol. Cell* **15**, 5383-5398. doi:10.1091/mbc.e04-08-0715
Homer, H. A., McDougall, A., Levasseur, M., Yallop, K., Murdoch, A. P. and Herbert, M. (2005). Mad2 prevents aneuploidy and premature proteolysis of cyclin B and securin during meiosis I in mouse oocytes. *Genes Dev.* **19**, 202-207. doi:10.1101/gad.328105
Jain, S., Wheeler, J. R., Walters, R. W., Agrawal, A., Barsic, A. and Parker, R. (2016). ATPase-modulated stress granules contain a diverse proteome and substructure. *Cell* **164**, 487-498. doi:10.1016/j.cell.2015.12.038
Kimura, H. and Cook, P. R. (2001). Kinetics of core histones in living human cells: little exchange of H3 and H4 and some rapid exchange of H2B. *J. Cell Biol.* **153**, 1341-1353. doi:10.1083/jcb.153.7.1341
Kondo, T., Kotani, T. and Yamashita, M. (2001). Dispersion of cyclin B mRNA aggregation is coupled with translational activation of the mRNA during zebrafish oocyte maturation. *Dev. Biol.* **229**, 421-431. doi:10.1006/dbio.2000.9990
Kotani, T. and Yamashita, M. (2002). Discrimination of the roles of MPF and MAP kinase in morphological changes that occur during oocyte maturation. *Dev. Biol.* **252**, 271-286. doi:10.1006/dbio.2002.0853
Kotani, T., Maehata, K. and Takei, N. (2017). Regulation of translationally repressed mRNAs in zebrafish and mouse oocytes. *Results Probl. Cell Differ.* **63**, 297-324. doi:10.1007/978-3-319-60855-6_13
Kotani, T., Yasuda, K., Ota, R. and Yamashita, M. (2013). Cyclin B1 mRNA translation is temporally controlled through formation and disassembly of RNA granules. *J. Cell Biol.* **202**, 1041-1055. doi:10.1083/jcb.201302139
Lancaster, A. K., Nutter-Upham, A., Lindquist, S. and King, O. D. (2014). PLAAC: a web and command-line application to identify proteins with prion-like amino acid composition. *Bioinformatics* **30**, 2501-2502. doi:10.1093/bioinformatics/btu310
Ledan, E., Polanski, Z., Terret, M. E. and Maro, B. (2001). Meiotic maturation of the mouse oocyte requires an equilibrium between cyclin B synthesis and degradation. *Dev. Biol.* **232**, 400-413. doi:10.1006/dbio.2001.0188
Lee, C. D. and Tu, B. P. (2015). Glucose-regulated phosphorylation of the PUF protein Puf3 regulates the translational fate of its bound mRNAs and association with RNA granules. *Cell Rep.* **11**, 1638-1650. doi:10.1016/j.celrep.2015.05.014
Lehmann, R. and Nüsslein-volhard, C. (1987). Involvement of the Pumilio gene in the transport of an abdominal signal in the Drosophila embryo. *Nature* **329**, 167-170. doi:10.1038/329167a0
Li, Y. R., King, O. D., Shorter, J. and Gitler, A. D. (2013). Stress granules as crucibles of ALS pathogenesis. *J. Cell Biol.* **201**, 361-372. doi:10.1083/jcb.201302044
Lin, Y., Protter, D. S. W., Rosen, M. K. and Parker, R. (2015). Formation and maturation of phase-separated liquid droplets by RNA-binding proteins. *Mol. Cell* **60**, 208-219. doi:10.1016/j.molcel.2015.08.018
Luong, X. G., Daldello, E. M., Rajkovic, G., Yang, C.-R. and Conti, M. (2020). Genome-wide analysis reveals a switch in the translational program upon oocyte meiotic resumption. *Nucleic Acids Res.* **48**, 3257-3276. doi:10.1093/nar/gkaa010
Maharana, S., Wang, J., Papadopoulos, D. K., Richter, D., Pozniakovsky, A., Poser, I., Bickle, M., Rizk, S., Guillen-Boixet, J., Franzmann, T. M. et al. (2018). RNA buffers the phase separation behavior of prion-like RNA binding proteins. *Science* **360**, 918-921. doi:10.1126/science.aar7366
Mak, W., Fang, C., Holden, T., Dratver, M. B. and Lin, H. (2016). An important role of Pumilio 1 in regulating the development of the mammalian female germline. *Biol. Reprod* **94**, 134. doi:10.1095/biolreprod.115.137497
Martin, K. C. and Ephrussi, A. (2009). mRNA localization: gene expression in the spatial dimension. *Cell* **136**, 719-730. doi:10.1016/j.cell.2009.01.044
Masui, Y. and Clarke, H. J. (1979). Oocyte maturation. *Int. Rev. Cytol* **57**, 185-282. doi:10.1016/S0074-7696(08)61464-3
McGrew, L. L., Dworkin-Rastl, E., Dworkin, M. B. and Richter, J. D. (1989). Poly(A) elongation during Xenopus oocyte maturation is required for translational recruitment and is mediated by a short sequence element. *Genes Dev.* **3**, 803-815. doi:10.1101/gad.3.6.803
Mendez, R. and Richter, J. D. (2001). Translational control by CPEB: a means to the end. *Nat. Rev. Mol. Cell Biol.* **2**, 521-529. doi:10.1038/35080081
Mikl, M., Vendra, G. and Kiebler, M. A. (2011). Independent localization of MAP2, CaMKIIα and β-actin RNAs in low copy numbers. *EMBO Rep.* **12**, 1077-1084. doi:10.1038/embor.2011.149
Mili, S. and Macara, I. G. (2009). RNA localization and polarity: from A(PC) to Z(BP). *Trends Cell Biol.* **19**, 156-164. doi:10.1016/j.tcb.2009.02.001
Moissoglu, K., Yasuda, K., Wang, T., Chrisafis, G. and Mili, S. (2019). Translational regulation of protrusion-localized RNAs involves silencing and clustering after transport. *eLife* **8**, e44752. doi:10.7554/eLife.44752.039
Molliex, A., Temirov, J., Lee, J., Coughlin, M., Kanagaraj, A. P., Kim, H. J., Mittag, T. and Taylor, J. P. (2015). Phase separation by low complexity domains promotes stress granule assembly and drives pathological fibrillization. *Cell* **163**, 123-133. doi:10.1016/j.cell.2015.09.015
Murata, Y. and Wharton, R. P. (1995). Binding of pumilio to maternal hunchback mRNA is required for posterior patterning in Drosophila embryos. *Cell* **80**, 747-756. doi:10.1016/0092-8674(95)90353-4
Nabti, I., Marangos, P., Bormann, J., Kudo, N. R. and Carroll, J. (2014). Dual-mode regulation of the APC/C by CDK1 and MAPK controls meiosis I progression and fidelity. *J. Cell Biol.* **204**, 891-900. doi:10.1083/jcb.201305049
Nakahata, S., Katsu, Y., Mita, K., Inoue, K., Nagahama, Y., and Yamashita, M. (2001). Biochemical identification of Xenopus Pumilio as a sequence-specific cyclin B1 mRNA-binding protein that physically interacts with a Nanos homolog, Xcat-2, and a cytoplasmic polyadenylation element-binding protein. *J. Biol. Chem.* **276**, 20945-20953. doi:10.1074/jbc.M010528200
Nakahata, S., Kotani, T., Mita, K., Kawasaki, T., Katsu, Y., Nagahama, Y. and Yamashita, M. (2003). Involvement of Xenopus Pumilio in the translational regulation that is specific to cyclin B1 mRNA during oocyte maturation. *Mech. Dev.* **120**, 865-880. doi:10.1016/S0925-4773(03)00160-6
Nott, T. J., Petsalaki, E., Farber, P., Jervis, D., Fussner, E., Plochowietz, A., Craggs, T. D., Bazett-Jones, D. P., Pawson, T., Forman-Kay, J. D. et al. (2015). Phase transition of a disordered nuage protein generates environmentally responsive membraneless organelles. *Mol. Cell* **57**, 936-947. doi:10.1016/j.molcel.2015.01.013
Ota, R., Kotani, T. and Yamashita, M. (2011a). Biochemical characterization of Pumilio1 and Pumilio2 in Xenopus oocytes. *J. Biol. Chem.* **286**, 2853-2863. doi:10.1074/jbc.M110.155523
Ota, R., Kotani, T. and Yamashita, M. (2011b). Possible involvement of Nemo-like kinase 1 in Xenopus oocyte maturation as a kinase responsible for Pumilio1, Pumilio2, and CPEB phosphorylation. *Biochemistry* **50**, 5648-5659. doi:10.1021/bi2002696
Pahlavan, G., Polanski, Z., Kalab, P., Golsteyn, R., Nigg, E. A. and Maro, B. (2000). Characterization of polo-like kinase 1 during meiotic maturation of the mouse oocyte. *Dev. Biol.* **220**, 392-400. doi:10.1006/dbio.2000.9656
Piqué, M., López, J. M., Foissac, S., Guigó, R. and Méndez, R. (2008). A combinatorial code for CPE-mediated translational control. *Cell* **132**, 434-448. doi:10.1016/j.cell.2007.12.038
Polanski, Z., Ledan, E., Brunet, S., Louvet, S., Verlhac, M. H., Kubiak, J. Z. and Maro, B. (1998). Cyclin synthesis controls the progression of meiotic maturation in mouse oocytes. *Development* **125**, 4989-4997.
Radford, H. E., Meijer, H. A. and de Moor, C. H. (2008). Translational control by cytoplasmic polyadenylation in Xenopus oocytes. *Biochim. Biophys. Acta* **1779**, 217-229. doi:10.1016/j.bbagrm.2008.02.002
Reijns, M. A., Alexander, R. D., Spiller, M. P. and Beggs, J. D. (2008). A role for Q/N-rich aggregation-prone regions in P-body localization. *J. Cell Sci.* **121**, 2463-2472. doi:10.1242/jcs.024976
Russo, A., Cirulli, C., Amoresano, A., Pucci, P., Pietropaolo, C. and Russo, G. (2008). cis-acting sequences and trans-acting factors in the localization of mRNA for mitochondrial ribosomal proteins. *Biochim. Biophys. Acta* **1779**, 820-829. doi:10.1016/j.bbagrm.2008.08.006
Saitoh, A., Takada, Y., Horie, M. and Kotani, T. (2018). Pumilio1 phosphorylation precedes translational activation of its target mRNA in zebrafish oocytes. *Zygote* **26**, 372-380. doi:10.1017/S0967199418000369
Salazar, A. M., Silverman, E. J., Menon, K. P. and Zinn, K. (2010). Regulation of synaptic Pumilio function by an aggregation-prone domain. *J. Neurosci.* **30**, 515-522. doi:10.1523/JNEUROSCI.2523-09.2010
Sheets, M. D., Fox, C. A., Hunt, T., Vande Woude, G. and Wickens, M. (1994). The 3'-untranslated regions of c-mos and cyclin mRNAs stimulate translation by regulating cytoplasmic polyadenylation. *Genes Dev.* **8**, 926-938. doi:10.1101/gad.8.8.926
Shiina, N. (2019). Liquid- and solid-like RNA granules form through specific scaffold proteins and combine into biphasic granules. *J Biol. Chem.* **294**, 3532-3548. doi:10.1074/jbc.RA118.005423
Smith, G. D., Sadhu, A., Mathies, S. and Wolf, D. P. (1998). Characterization of protein phosphatases in mouse oocytes. *Dev. Biol.* **204**, 537-549. doi:10.1006/dbio.1998.9043
Souquere, S., Beauclair, G., Harper, F., Fox, A. and Pierron, G. (2010). Highly ordered spatial organization of the structural long noncoding NEAT1 RNAs within paraspeckle nuclear bodies. *Mol. Biol. Cell* **21**, 4020-4027. doi:10.1091/mbc.e10-08-0690
Spassov, D. S. and Jurecic, R. (2003). The PUF family of RNA-binding proteins: does evolutionarily conserved structure equal conserved function? *IUBMB Life* **55**, 359-366. doi:10.1080/1521654031000160309 3
Susor, A., Jansova, D., Cerna, R., Danylevska, A., Anger, M., Toralova, T., Malik, R., Supolikova, J., Cook, M. S., Oh, J. S. et al. (2015). Temporal and spatial regulation of translation in the mammalian oocyte via the mTOR-eIF4F pathway. *Nat. Commun.* **6**, 6078. doi:10.1038/ncomms7078
Takei, N., Nakamura, T., Kawamura, S., Takada, Y., Satoh, Y., Kimura, A. P. and Kotani, T. (2018). High-sensitivity and high-resolution in situ hybridization of coding and long non-coding RNAs in vertebrate ovaries and testes. *Biol. Proced. Online* **20**, 6. doi:10.1186/s12575-018-0071-z
Tay, J., Hodgman, R. and Richter, J. D. (2000). The control of cyclin B1 mRNA translation during mouse oocyte maturation. *Dev. Biol.* **221**, 1-9. doi:10.1006/dbio.2000.9669

Trcek, T., Grosch, M., York, A., Shroff, H., Lionnet, T. and Lehmann, R. (2015). Drosophila germ granules are structured and contain homotypic mRNA clusters. *Nat. Commun.* **6**, 7962. doi:10.1038/ncomms8962

Tsutsumi, M., Muto, H., Myoba, S., Kimoto, M., Kitamura, A., Kamiya, M., Kikukawa, T., Takiya, S., Demura, M., Kawano, K. et al. (2016). In vivo fluorescence correlation spectroscopy analyses of FMBP-1, a silkworm transcription factor. *FEBS Open Bio.* **6**, 106-125. doi:10.1002/2211-5463.12026

Vogler, T. O., Wheeler, J. R., Nguyen, E. D., Hughes, M. P., Britson, K. A., Lester, E., Rao, B., Betta, N. D., Whitney, O. N., Ewachiw, T. E. et al. (2018). TDP-43 and RNA form amyloid-like myo-granules in regenerating muscle. *Nature* **563**, 508-513. doi:10.1038/s41586-018-0665-2

Wang, J. T., Smith, J., Chen, B. C., Schmidt, H., Rasoloson, D., Paix, A., Lambrus, B. G., Calidas, D., Betzig, E. and Seydoux, G. (2014). Regulation of RNA granule dynamics by phosphorylation of serine-rich, intrinsically disordered proteins in C. *elegans*. *eLife* **3**, e04591. doi:10.7554/eLife.04591

Weber, S. C. and Brangwynne, C. P. (2012). Getting RNA and protein in phase. *Cell* **149**, 1188-1191. doi:10.1016/j.cell.2012.05.022

West, J. A., Mito, M., Kurosaka, S., Takumi, T., Tanegashima, C., Chujo, T., Yanaka, K., Kingston, R. E., Hirose, T., Bond, C. et al. (2016). Structural, super-resolution microscopy analysis of paraspeckle nuclear body organization. *J. Cell Biol.* **214**, 817-830. doi:10.1083/jcb.201601071

Wickens, M., Bernstein, D. S., Kimble, J. and Parker, R. (2002). A PUF family portrait: 3'UTR regulation as a way of life. *Trends Genet.* **18**, 150-157. doi:10.1016/S0168-9525(01)02616-6

Winata, C. L. and Korzh, V. (2018). The translational regulation of maternal mRNAs in time and space. *FEBS Lett.* **592**, 3007-3023. doi:10.1002/1873-3468.13183

Zhang, B., Gallegos, M., Puoti, A., Durkin, E., Fields, S., Kimble, J. and Wickens, M. P. (1997). A conserved RNA-binding protein that regulates sexual fates in the C. elegans hermaphrodite germ line. *Nature* **390**, 477-484. doi:10.1038/37297

Zhang, M., Chen, D., Xia, J., Han, W., Cui, X., Neuenkirchen, N., Hermes, G., Sestan, N. and Lin, H. (2017). Post-transcriptional regulation of mouse neurogenesis by Pumilio proteins. *Genes Dev.* **31**, 1-16. doi:10.1101/gad.295980.117

Supplemental Figures

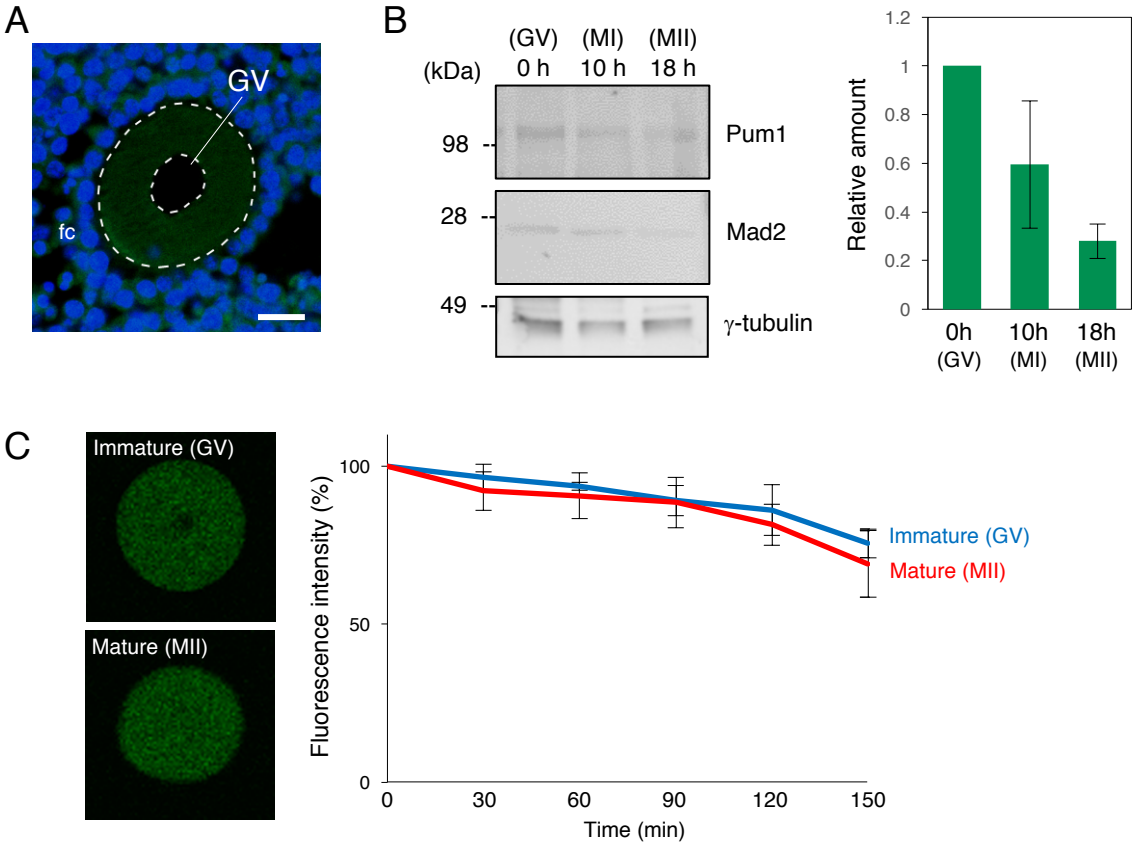

Fig. S1. Expression of *Mad2* mRNA and Mad2 protein. (A) FISH analysis of *Mad2* mRNA (green). DNA is shown in blue. No signal was detected by using the antisense RNA probe for long *Mad2*. (B) Effect of puromycin on Mad2 protein accumulation. (left) Immunoblotting of Pum1, Mad2 and γ-tubulin in oocytes incubated with puromycin at 0, 10, and 18 h after resumption of meiosis. (right) Quantitative analysis of Mad2 protein (mean ± SD; n = 2). The intensities of Mad2 were normalized by that of γ-tubulin. (C) Time course analysis of GFP-Mad2 fluorescence after treated with puromycin (mean ± SD; n = 3). GV, germinal vesicle; fc, follicle cells. Bars: 20 μm.

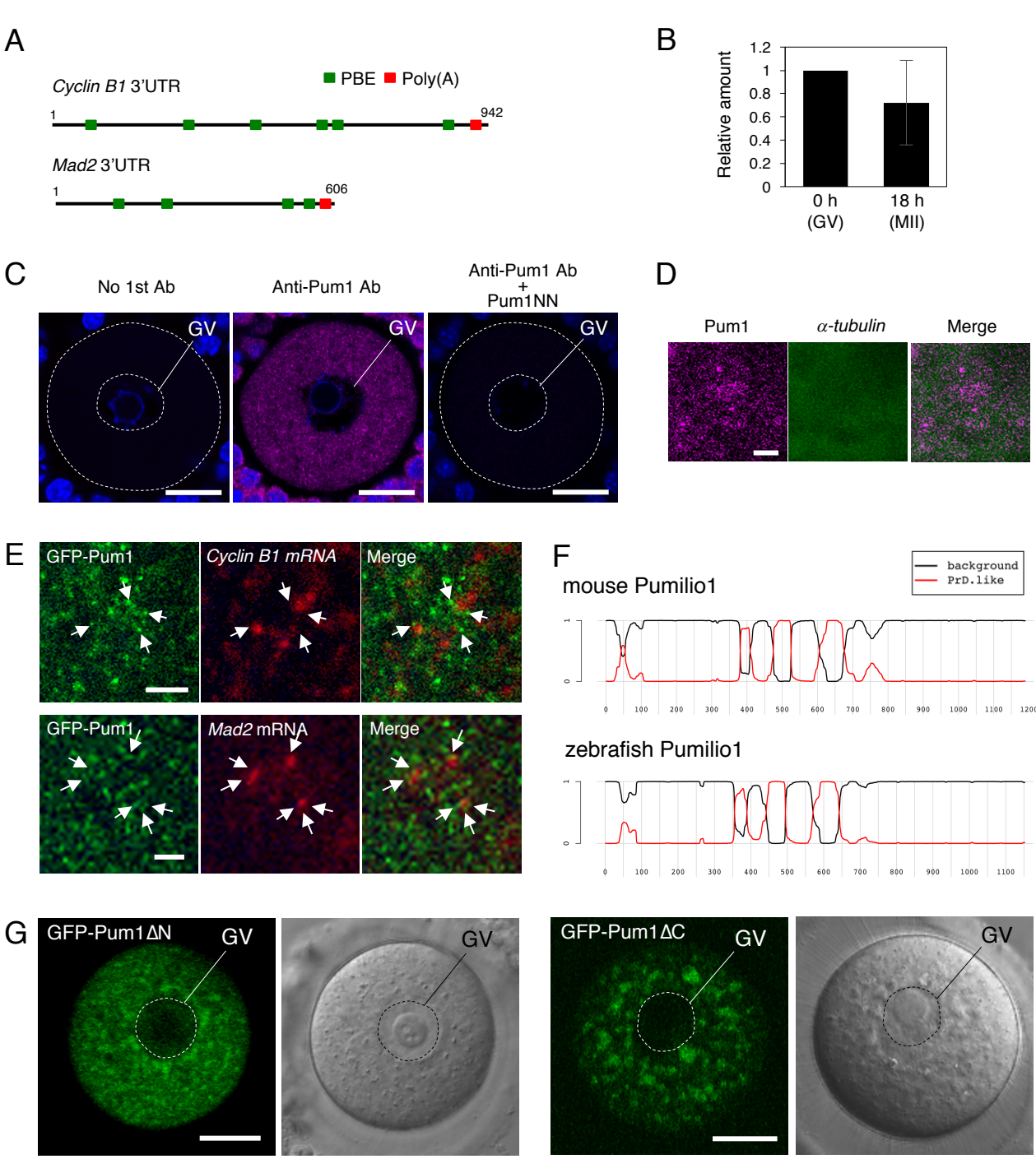

Fig. S2. Distribution of Pum1, GFP-Pum1 and mRNAs. (A) Schematic diagrams of mouse *Cyclin B1* and *Mad2* 3'UTRs. Green rectangles indicate putative Pumilio-binding elements (PBEs), and red rectangles indicate the poly(A) signal. (B) Quantitative PCR for *Mad2* mRNA in oocytes at 0 and 18 h after resumption of meiosis (mean ± SD; n = 3). (C) Immunofluorescence of Pum1 (magenta) in immature oocytes. DNA is shown in blue. Mouse ovary sections were reacted with buffer only (No 1st Ab), anti-Pum1 antibody (Anti-Pum1 Ab), or anti-Pum1 antibody incubated with recombinant Pum1 (Anti-Pum1 Ab + Pum1NN). (D) FISH analysis of *α-tubulin* mRNA (green) and immunostaining of Pum1 (magenta) in immature oocytes. (E) FISH analysis of *Cyclin B1* (top) and *Mad2* mRNA (bottom) and immunostaining of GFP in oocytes expressing GFP-Pum1. Arrows indicate aggregates of GFP-Pum1 surrounding *Cyclin B1* or *Mad2* RNA granules. Similar results were obtained from two independent experiments. (F) Identification of prion-like domains by using the PLAAC web application (http://plaac.wi.mit.edu/.). (G) Distribution of GFP-Pum1 ΔN and GFP-Pum1 ΔC in immature oocytes. Similar results were obtained from six independent experiments. GV, germinal vesicle. Bar: 20 μm in C and G, 2 μm in D and E.

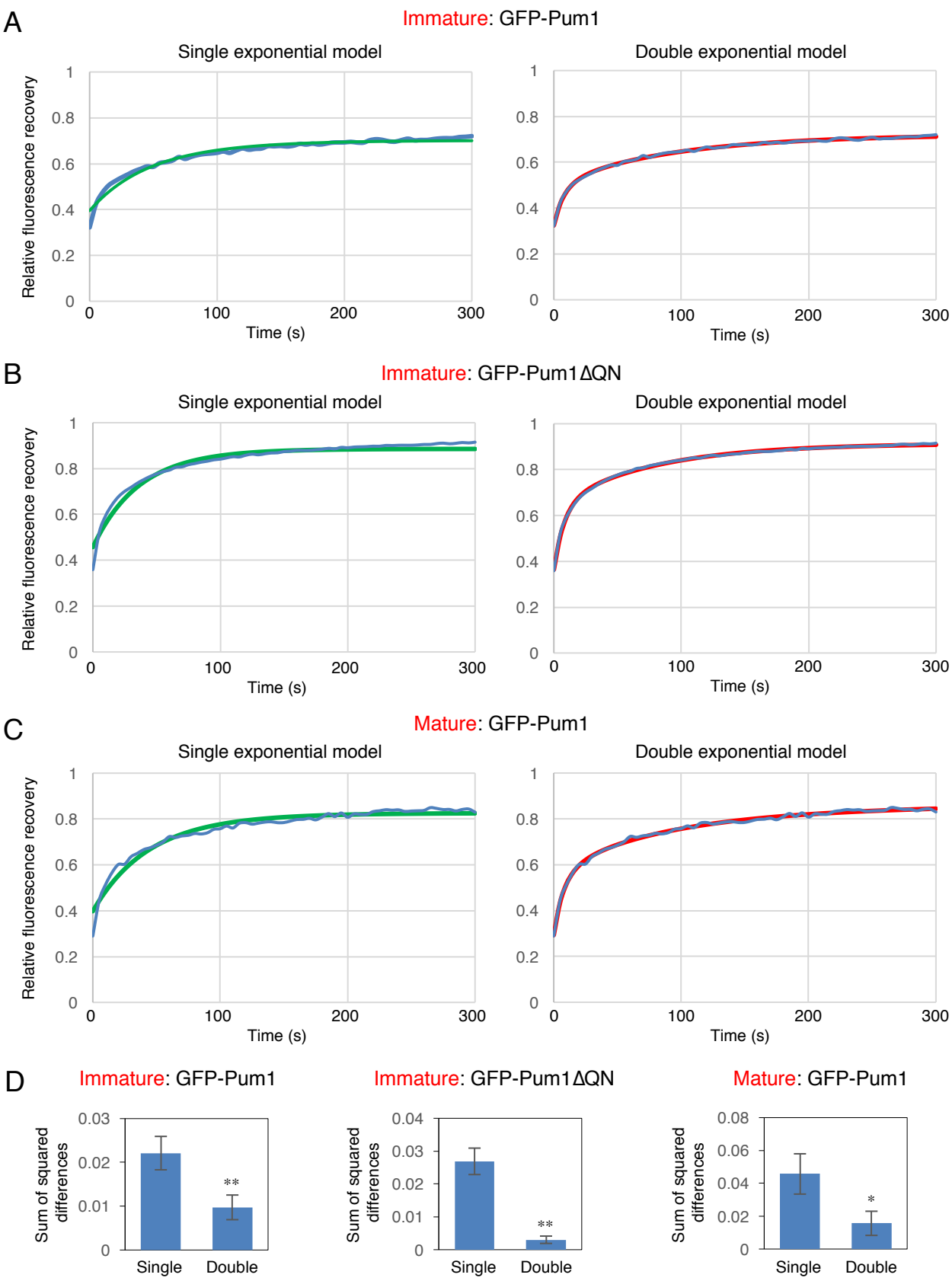

Fig. S3. FRAP analysis of GFP-Pum1 and GFP-Pum1ΔQN. (A) The average of fluorescence recovery curves (blue) of GFP-Pum1 in immature oocytes with the fittings to single (left, green) or double (right, magenta) exponential model. (B) The average of fluorescence recovery curves (blue) of GFP-Pum1ΔQN in immature oocytes with the fittings to single (left, green) or double (right, magenta) exponential model. (C) The average of fluorescence recovery curves (blue) of GFP-Pum1 in mature oocytes with the fittings to single (left, green) or double (right, magenta) exponential model. (D) Sum of squared differences between the fluorescence recovery curves and the single (Single) or double (Double) exponential model (mean ± SD). *t*-test: $*P < 0.05$, $**P < 0.01$.

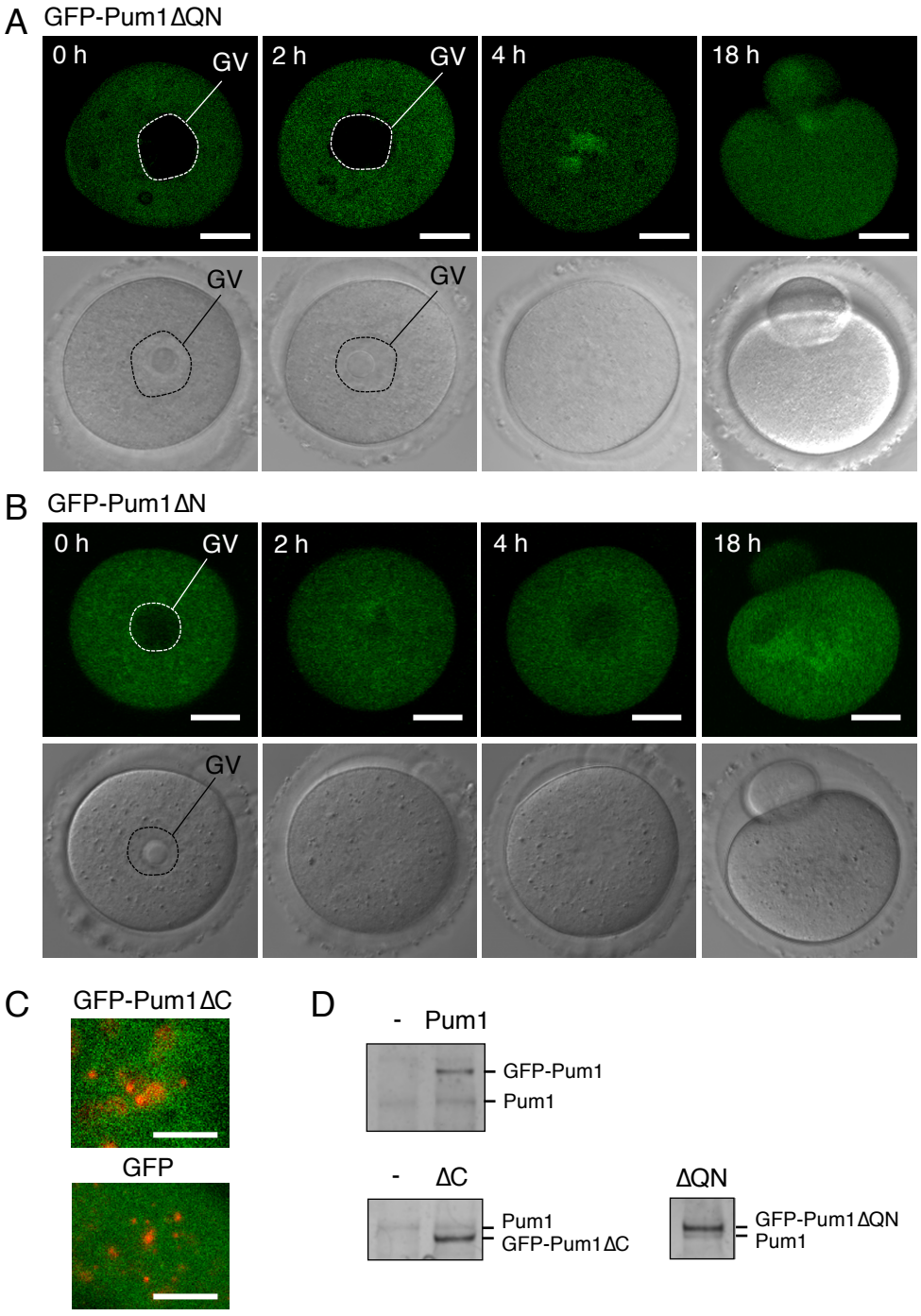

Fig. S4. Time course of GFP-Pum1ΔQN and GFP-Pum1ΔN during oocyte maturation. (A) Time course of GFP-Pum1ΔQN at 0, 2, 4 and 18 h after resumption of meiosis. (B) Time course of GFP-Pum1ΔN at 0, 2, 4 and 18 h after resumption of meiosis. Similar results were obtained from two independent experiments. (C) FISH analysis of *Cyclin B1* (red) mRNA and immunostaining of GFP-Pum1ΔC or GFP (green) in immature oocytes. (D) Immunoblotting of Pum1 in oocytes not injected (-) and injected with GFP-Pum1 (Pum1), GFP-Pum1ΔC (ΔC) and GFP-Pum1ΔQN (ΔQN). GFP-Pum1ΔN is unable to be detected since the anti-Pum1 antibody recognizes the region delated in this mutant Pum1. Bars: 20 μm in A and B, 5 μm in C.

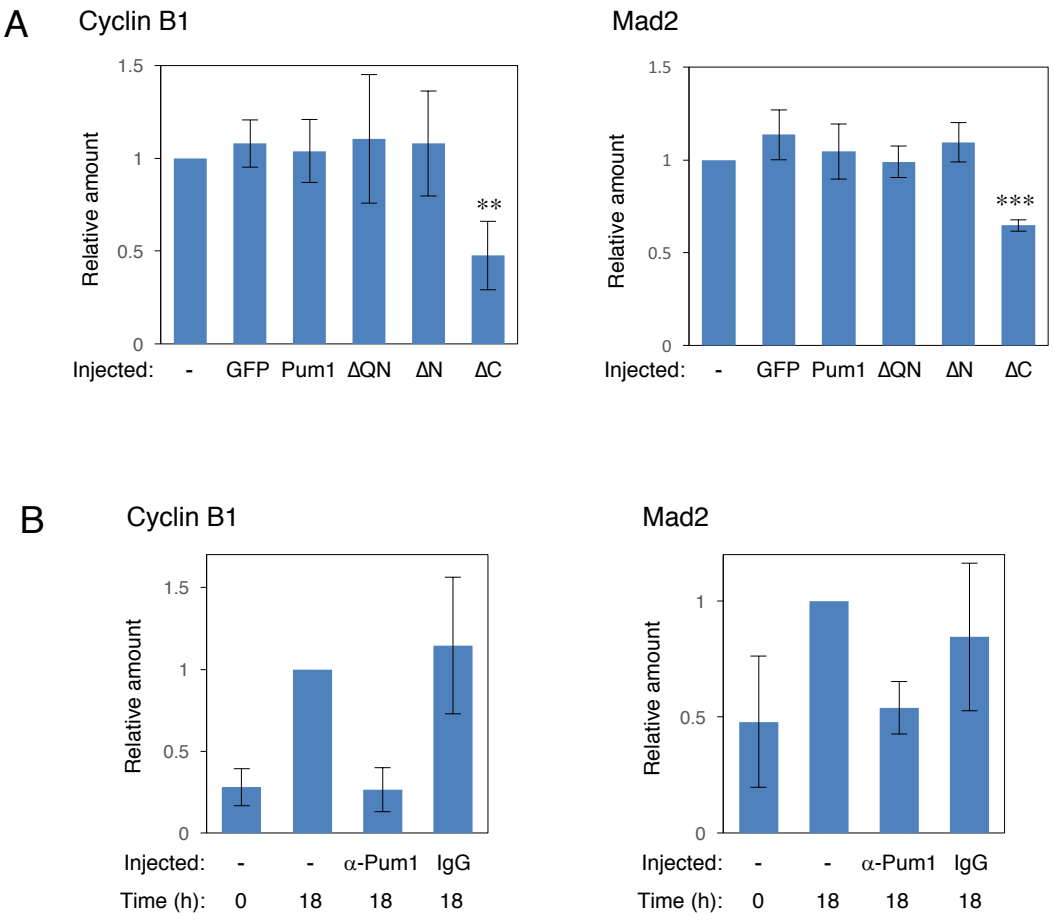

Fig. S5. Quantitative analyses of Cyclin B1 and Mad2 proteins. (A) Quantitative analysis of Cyclin B1 and Mad2 in oocytes not injected (-) and injected with GFP, GFP-Pum1 (Pum1), GFP-Pum1ΔQN (ΔQN), GFP-Pum1ΔN (ΔN), and GFP-Pum1ΔC (ΔC) (mean ± SD; n = 3). *t*-test: $^{**}P < 0.01$, $^{***}P < 0.001$. (B) Quantitative analysis of Cyclin B1 and Mad2 in oocytes not injected (-) and injected with anti-Pum1 antibody (α-Pum1) or control IgG (IgG) (mean ± SD; n = 2).

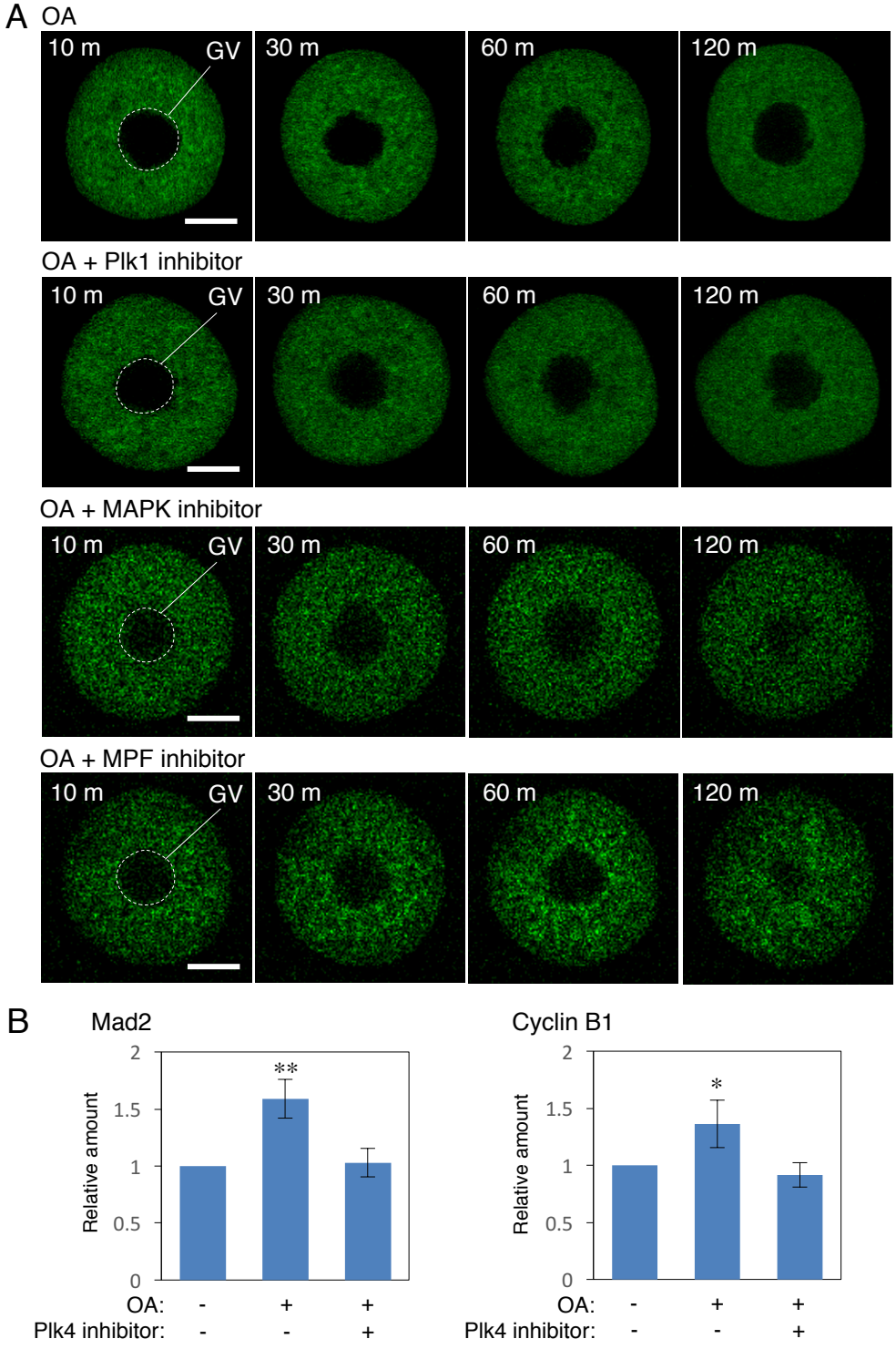

Fig. S6. Time course of GFP-Pum1 after OA treatment. (A) Time course of GFP-Pum1 in oocytes treated with OA, OA and Plk1 inhibitor, OA and MAPK inhibitor, or OA and MPF inhibitor 0-120 min after treatment. Similar results were obtained in 6 oocytes from two independent experiments. GV, germinal vesicle. Bars: 20 μm. (B) Quantitative analysis of Mad2 and Cyclin B1 in oocytes treated with (+) and without (-) OA or Plk4 inhibitor 120 min after resumption of meiosis (mean ± SD; n = 3). *t*-test: *$P < 0.05$, **$P < 0.01$.